NUMERICAL SIMULATION
OF
CRITICAL LAYER EVOLUTION

by

C. Harold Ritchie

A thesis submitted to the Faculty of Graduate Studies and Research in partial fulfillment of the requirements for the degree of Master of Science

Department of Meteorology
McGill University
Montreal, Quebec

July, 1978

ABSTRACT

The non-divergent barotropic vorticity equation is integrated numerically in order to investigate a potential resonance mechanism for Rossby waves on a shear flow in the presence of a nonlinear critical layer. The numerical model, which uses a mixture of spectral and finite element techniques, simulates the propagation of a weakly forced Rossby wave on a semi-infinite beta plane. It is found that a large amplitude response can be obtained by "tuning" the geometry of the flow and that there is an associated increase in the thickness of the critical layer. The logarithmic phase shift is also investigated. It appears to develop an imaginary part as the nonlinearities come into force.

RESUME

Afin d'étudier un mécanisme de résonnance pour les ondes de Rossby en présence d'une couche critique non-linéaire, l'équation non-divergente du tourbillon barotrope est solutionnée à l'aide d'un modèle numérique. Le modèle numérique, qui se sert de la méthode spectrale et des éléments finis, simule la propagation d'une onde de Rossby faiblement entretenue à la frontière nord, sur un plan beta semi-infini. On démontre qu'une réponse de grande amplitude peut être obtenue en changeant la géométrie de l'écoulement et que ceci correspond à une augmentation de l'épaisseur de la couche critique. On étudie aussi le "logarithmic phase shift". Une partie imaginaire semble se développer quand les termes non-linéaires deviennent importants.

ACKNOWLEDGEMENTS

The author wishes to thank his thesis supervisor, Dr. Tom Warn, for his guidance and enthusiasm in all aspects of this project. He is also grateful to the Atmospheric Environment Service for their financial support and the computing facilities and assistance provided by the Division de Recherche en Prévision Numérique. Particular thanks goes to Dr. Andrew Staniforth for his help in the application of the finite element method to this problem.

TABLE OF CONTENTS

LIST OF FIGURES

LIST OF TABLES

CHAPTER 1. INTRODUCTION

The main objective of this thesis is to investigate a potential resonance mechanism for Rossby waves on a shear flow in the presence of a nonlinear critical layer.

Although synoptic scale waves are largely responsible for the day to day variations in the weather, the planetary scale waves play a major role in steering the synoptic waves and thus controlling the weather on the longer time scales. Despite the importance of the planetary waves there are still many aspects of their behavior which are poorly understood and poorly forecast. One such phenomenon is the amplification of nearly stationary high pressure systems which deflect travelling cyclones from their usual paths and often result in significant weather anomalies. Recently it has been argued (Tung, 1977) that a theory of resonant stationary waves could account for the creation of such "blocking patterns".

The classical resonance phenomenon arises from linearized theory and occurs when one of the normal modes in a physical system is forced in some way. However, there are some difficulties in applying linearized resonance theory to the atmosphere. The prime candidates for atmospheric forcing are the land-sea thermal contrasts and the topographic forcing -- both of which are geographically fixed and hence have zero forcing frequency. The linearized, steady, inviscid version of the equation governing the propagation of Rossby waves has a singularity where the Doppler shifted frequency of the disturbance vanishes. This location is called the "critical level"

and, in the case of zero forcing frequency, is the line separating the westerlies from the easterlies. In order to overcome the local failure of the simplified governing equation it is necessary to re-introduce at least one of the neglected processes -- namely, time dependence, viscosity, or nonlinearity. The region (surrounding the critical level) in which these processes are important is called the "critical layer". Thus the flow can be divided into three regions -- two regions (one north of the critical layer and one south) in which the linearized, steady, inviscid equation is a good approximation, and the critical layer in which some of these processes must be retained. One of the main objectives of critical layer research has been to connect the solutions north of the critical layer to the solutions to the south by examining the processes within the critical layer. Many of the results of this research have been expressed in terms of the "logarithmic phase shift", θ, which is related to the resonance problem by the fact that its real part must be zero if the system is to have a normal mode. It has been found that if viscosity (see Lin, 1967) or time dependence (Dickinson, 1970) is re-introduced θ assumes the value $-\pi$ and, consequently, no normal modes are allowed if the linearization assumption is retained. Thus the classical resonance mechanism is precluded.

The only hope of having normal modes rests with the nonlinearities. Various researchers have re-introduced nonlinearities by using perturbation techniques appropriate for small disturbances, with ϵ frequently being a small parameter proportional to the perturbation amplitude. Using this approach Benney and Bergeron (1969) and Davis (1969) found that for steady flows the relative importance of viscous

and nonlinear effects in the critical layer is given by a parameter $\lambda = \nu/\epsilon^{3/2}$ (ν being the kinematic coefficient of viscosity). θ has the value 0 in the limit as λ goes to zero. Haberman (1972) studied the steady problem for the full range of λ and found θ as a smooth function of λ_c, which depends on λ and the perturbation amplitude at the critical level, with $\theta = 0$ for $\lambda_c = 0$ and $\theta = -\pi$ as $\lambda_c \to \infty$ in keeping with the previously mentioned steady state results. Some of the difficulties which occurred in the above nonlinear analyses have been resolved recently by Brown and Stewartson (1978). The conclusions concerning the behavior of θ remain unchanged -- in particular its real part is zero in the steady, nonlinear, inviscid limit.

The effect of time dependence on the nonlinear problem has also been examined. Warn and Warn (1978) used perturbation techniques to derive a time dependent, nonlinear, inviscid critical layer equation which they solved numerically and found that θ is a function of the slow time scale $\tau = \epsilon^{1/2} t$. Stewartson (1978) obtained analytic solutions to the critical layer equation under certain limiting conditions. Béland (1976) has also studied time dependence by taking a fully numerical approach. His results for a series of integrations of the time dependent, inviscid problem for small amplitude disturbances are in accord with Warn and Warn's findings and also show that many of the previous steady state results can be obtained from the initial value problem. Béland (1978) examined the effect of viscosity and showed that long time integrations could also produce results in qualitative agreement with the steady state behavior reported by Haberman. Thus it has been shown that nonlinearities, whether

in the steady state or time dependent problem, can produce a logarithmic phase shift with a zero real part -- which is a necessary condition for the existence of normal modes.

The existence of normal modes does not in itself guarantee that resonance will occur -- the normal modes appear only in a nonlinear problem and the conclusions of linear theory (for example, that forcing a normal mode will produce a resonance) must be used with great caution. Tung (1977) investigated resonance using a time dependent, damped, linear model with the critical layer treated as a reflecting surface. Nevertheless, it still has not been demonstrated that a large response can actually be produced in a transient, nonlinear, viscous problem. Furthermore, it is not clear how the critical layer should behave during the evolution of any such resonant response. These are the two main points examined in this thesis.

To focus attention on the nonlinear mechanism and facilitate interpretation we use a simple model which contains the essential dynamics and in which the role of the nonlinearities is easily identified. Many of the results quoted above have been found using techniques which are not appropriate for large amplitude disturbances. Such techniques could become invalid as the wave resonates and consequently we turn to a numerical approach which is free of these limitations. Specifically, the non-divergent barotropic vorticity equation is modelled using a mixture of spectral and finite element techniques. This model is similar to the one used by Béland with the main change being the replacement of the standard finite differences by the finite element method. Variable resolution can be accurately incorporated in the finite element method, leading to increased computational

efficiency by resolving the short scales of motion in the critical layer without requiring unnecessarily high resolution elsewhere.

In this thesis we restrict ourselves to initial shear flows $\bar{u}(y)$ that are monotonic in y so that steady waves possess only one critical layer. We also exclude the special case in which the gradient of the mean absolute vorticity $\beta - \frac{d^2\bar{u}}{dy^2}$ also vanishes at the critical level.

CHAPTER 2. THEORETICAL FORMULATION

2.1 The model equations

We shall study the evolution of two-dimensional Rossby waves generated by a small stationary forcing (proportional to ϵ) in mid-latitudes and propagating southward in the semi-infinite domain $-\infty < y \leq y_m$ on an initial shear flow $\bar{u}(y)$. The beta plane approximation will be made and the flow will be periodic in x which corresponds to a latitude circle. The governing equation is the non-dimensional, non-divergent barotropic vorticity equation

$$\frac{\partial}{\partial t}\nabla^2 \Psi + \Psi_x \nabla^2 \Psi_y - \Psi_y \nabla^2 \Psi_x + \beta \Psi_x = \nu \nabla^4 \Psi \qquad (2.1).$$

Ψ is the streamfunction, related to the longitudinal and transverse velocity components through $u = -\Psi_y$, $v = \Psi_x$, β is the constant beta plane parameter and ν is the kinematic coefficient of viscosity. The non-dimensional quantities are related to their dimensional (primed) counterparts by

$$(x, y, t) = (x'/L_x,\ y'/L,\ U_s t'/L_x)$$

$$(\Psi,\ \beta,\ \nu) = (\Psi'/(U_s L),\ L^2 \beta'/U_s,\ L_x \nu'/(L^2 U_s))$$

where L and U_s are typical length and velocity scales determined by the background velocity profile and $L_x = a \cos \phi_0$ with a being the

mean radius of the earth and ϕ_0 a typical latitude. Thus x will vary from 0 to 2π around a latitude circle. Also

$$\nabla^2 = \alpha^2 \frac{\partial^2}{\partial x^2} + \frac{\partial^2}{\partial y^2} \qquad \alpha = L/L_x .$$

The initial condition is taken to be $\Psi(x, y, 0) = -\int^y \bar{u}(\xi)d\xi$ and the northern boundary condition is a stationary sinusoidal forcing of the transverse velocity for integral wavenumber k

$$\Psi_x(x, y_m, t) = -2\epsilon k \sin(kx) ,$$

simulating the presence in mid-latitudes of a weak Rossby wave which will propagate southward. Introducing the perturbation streamfunction Φ and perturbation vorticity ζ such that

$$\Psi = -\int^y \bar{u}(\xi)\,d\xi + \epsilon\,\Phi(x, y, t)$$

$$\zeta = \nabla^2 \Phi \qquad (2.2)$$

results in

$$\zeta_t + \bar{u}(y)\zeta_x + (\beta - \frac{d^2\bar{u}}{dy^2})\Phi_x + \epsilon(\Phi_x \zeta_y - \Phi_y \zeta_x)$$

$$= \nu\nabla^2\zeta - \frac{\nu}{\epsilon}\frac{d^3\bar{u}}{dy^3} \qquad (2.3)$$

with initial and northern boundary conditions

$$\Phi(x, y, 0) = 0$$

$$\Phi_x = -2k \sin(kx) \qquad (2.4)$$

The term $-\nu/\epsilon \frac{d^3\bar{u}}{dy^3}$ appears on the right hand side of equation (2.3) because $-\int^y \bar{u}(\xi)d\xi$ is not an exact solution of the steady linear viscous equation.

Notice that ϵ is a measure of the strength of the nonlinearities in equation (2.3). The unbounded domain in y will be simulated by using a finite computational domain $y_1 \le y \le y_m$ together with a radiation condition at y_1. This will be discussed in the next chapter.

2.2 Critical layers and resonance

The steady, linearized, inviscid version of equation (2.3) is

$$\zeta_x + \frac{\beta - \bar{u}''(y)}{\bar{u}(y)} \Phi_x = 0 \qquad \text{where } ' \text{ denotes } \frac{d}{dy}.$$

If $\Phi = \phi_k(y) e^{ikx}$ then

$$\frac{d^2\phi_k}{dy^2} + \left(\frac{\beta - \bar{u}''(y)}{\bar{u}(y)} - \alpha^2 k^2 \right) \phi_k = 0 . \qquad (2.5)$$

This equation has a regular singularity at a value y_c where $\bar{u}(y_c) = 0$ and using the method of Frobenius it is possible to find solutions

$$\phi_k(y) = a_k^+ \phi_{a_k}(y) + b_k^+ \phi_{b_k}(y) \qquad y > y_c$$

$$= a_k^- \phi_{a_k}(y) + b_k^- \phi_{b_k}(y) \qquad y < y_c$$

where

$$\phi_{a,k} = (y - y_c) - \frac{(\beta - \bar{u}_c'')}{2\bar{u}_c'} (y - y_c)^2 + \cdots \qquad (2.6)$$

$$\phi_{b,k} = 1 + \left\{ \alpha^2 k^2 + \frac{\bar{u}_c'''}{\bar{u}_c'} + \frac{(\beta - \bar{u}_c'')\bar{u}_c''}{2\bar{u}_c'^2} - \frac{3}{2}\left[\frac{\beta - \bar{u}_c''}{\bar{u}_c'}\right]^2 \right\} \frac{(y - y_c)^2}{2}$$

$$+ \cdots - \frac{(\beta - \bar{u}_c'')}{\bar{u}_c'} \phi_{a,k} \ln |y - y_c| \qquad (2.7).$$

The subscript "c" denotes evaluation at y_c. Notice that different coefficients are allowed north and south of y_c and that ϕ_{b_k} contains a term $(y-y_c)\ln|y-y_c|$ which vanishes at y_c but produces a $\ln|y-y_c|$ behavior when differentiated. Thus $\phi_{a_k}(y_c) = 0$, $\phi_{b_k}(y_c) = 1$, but $\frac{d\phi_{b_k}}{dy}$ has a logarithmic singularity at y_c and hence equation (2.5) cannot describe the flow at y_c, the "critical level" for this model. To overcome this failure it is necessary to re-introduce at least one of the neglected processes (time dependence, nonlinearity, or viscosity) in the vicinity of y_c, which is referred to as the "critical layer". Thus the flow can be divided into three regions; the critical layer and two "outer regions" to the north and south where $a_k^{\pm}\phi_{a_k}(y) + b_k^{\pm}\phi_{b_k}(y)$ are good approximations. A main goal of critical layer research has been to find connection formulae relating a_k^+, a_k^-, b_k^+, and b_k^- by examining the processes within the critical layer. The available results provide a description of many of the salient aspects of the critical layer evolution and suggest a potential resonance mechanism for Rossby waves.

In all cases it has been found that one connection formula is $b_k^+ = b_k^-$, while the relation between a_k^+ and a_k^- depends upon which process dominates the critical layer. Defining

$$a_k^+ - a_k^- = [a_k] = i\,\frac{(\beta - \bar{u}_c'')}{|\bar{u}_c'|}\,b_k\,\theta \qquad (2.8)$$

the steady, linearized, inviscid solution can be written as

$$\phi_k(y) = a_k^+\,\phi_{a_k}(y) + b_k\,\hat{\phi}_{b_k}(y)$$

where

$$\hat{\phi}_{bk}(y) = 1 + \left\{\alpha^2 k^2 + \frac{\bar{u}_c'''}{\bar{u}_c'} + \frac{(\beta-\bar{u}_c'')\bar{u}_c''}{2\,\bar{u}_c'^2} - \frac{3}{2}\left(\frac{\beta-\bar{u}_c''}{\bar{u}_c'}\right)^2\right\}\frac{(y-y_c)^2}{2}$$

$$+ \ldots - \frac{(\beta-\bar{u}_c'')}{\bar{u}_c'}\,\phi_{ak}\ln(y-y_c)$$

with the understanding that for $y<y_c$

$$\ln(y-y_c) = \ln|y-y_c| + i\theta\,\mathrm{sgn}(\bar{u}_c').$$

θ is called the "logarithmic phase shift" and its real part θ_R can be related to the jump in the Reynolds stress $[R]$ across the critical layer via

$$\theta_R = \frac{|\bar{u}_c'|\,[R]}{2k(\beta-\bar{u}_c'')\,|b_k|^2} \qquad (2.9).$$

The early phase in the evolution of the initial value problem is described by linear inviscid processes as examined by Dickinson (1970), with the thickness of the critical layer decreasing like $1/t$ and θ assuming the value $-\pi$. If no other process is present the critical layer continues to collapse and as $t\to\infty$ the singularity of the steady problem is recovered. If viscosity is dominant, for $t\sim O(\nu^{-1/3})$ the thickness will equilibrate at $O(\nu^{1/3})$. θ will remain at $-\pi$ and the steady, linear, viscous state described by Lin (1967) will result. If nonlinearities (as opposed to viscosity) are present θ is found to be a function of the long time scale $\tau = \epsilon^{1/2}t$ (Stewartson, 1978; Warn and Warn, 1978). The thickness equilibrates at $O(\epsilon^{1/2})$ with θ vanishing as $\tau\to\infty$ as in the steady, nonlinear state examined by

Benney and Bergeron (1969) and Davis (1969). When all three processes are present the relative importance of the viscosity and nonlinearity is given by $\lambda = \nu/\epsilon^{3/2}$, the cube of the ratio of the respective layer thicknesses, and the steady state value of θ is a function of the parameter λ_c (proportional to $\lambda/|b_k|^{3/2}$) which varies smoothly from $-\pi$ for $\lambda_c \to \infty$ to 0 for $\lambda_c = 0$ (Haberman, 1972; Béland, 1978). These results can be combined to provide some insight into a potential resonance mechanism for Rossby waves, but first it should be mentioned that the thickness of the steady nonlinear critical layer is actually $O(\epsilon^{1/2}|b_k|^{1/2})$ where b_k has been assumed to be $O(1)$ in the preceding discussion.

Consider a wind profile $\bar{u}(y) = y$, together with the "long wave limit" $|\alpha^2 k^2| \ll |\beta/y|$. Then equation (2.5) becomes

$$\frac{d^2\phi}{dy^2} + \frac{\beta}{y}\phi = 0 , \qquad (2.10)$$

which is a transformed Bessel's equation (Dickinson, 1968). It is possible to identify the Bessel function solutions with linear combinations of $\phi_{a_k}(y)$ and $\phi_{b_k}(y)$. Thus for $y>0$

$$\phi = \left\{\frac{q_k^+}{\beta} + b_k(2\gamma + \ln\beta - 1)\right\}\sqrt{\beta y}\, J_1(2\sqrt{\beta y}) - b_k\pi\, Y_1(2\sqrt{\beta y})$$

and for $y<0$

$$\phi = \left\{b_k(1-2\gamma-\ln\beta) - \frac{q_k^-}{\beta}\right\}\sqrt{-\beta y}\, I_1(2\sqrt{-\beta y}) + 2b_k\sqrt{-\beta y}\, K_1(2\sqrt{-\beta y}).$$

Here γ is Euler's constant. For a bounded solution as $y \to -\infty$ the

coefficient of $I_1(2\sqrt{-\beta y})$ must be zero. Also using definition (2.8) the solution for $y>0$ becomes

$$\phi(y) = b_k \sqrt{\beta y}\left\{ i\theta J_1(2\sqrt{\beta y}) - \pi Y_1(2\sqrt{\beta y})\right\}. \quad (2.11)$$

Thus $\phi(y)$ is proportional to b_k which is determined from the forcing boundary condition (2.4) in the north, that is, $\phi(y_m) = 1$, or

$$b_k = \frac{1}{\sqrt{\beta y_m}\left\{ i\theta J_1(2\sqrt{\beta y_m}) - \pi Y_1(2\sqrt{\beta y_m})\right\}} \quad . \quad (2.12)$$

If the combination βy_m is chosen such that $Y_1(2\sqrt{\beta y_m}) = 0$ and $\theta \to 0$ as in the nonlinear limit, equations (2.11) and (2.12) show that $\phi(y)$ would become unbounded; that is, a resonance would result. y_m is the distance between the forcing boundary and the critical level, so changing βy_m to produce a large b_k could be interpreted as looking for a resonance by "tuning" the geometry of the flow. This strongly suggests that it should be possible to resonantly excite a wave with a nonlinear critical layer. Notice also that if a complex θ is allowed, $\theta = \theta_R + i\theta_I$, b_k becomes unbounded if $\theta_R = 0$ and $\theta_I = -\frac{\pi Y_1(2\sqrt{\beta y_m})}{J_1(2\sqrt{\beta y_m})}$. As will be seen later, θ_I could play an important role in the resonance mechanism. Since the thickness of the critical layer is $O(\epsilon^{1/2}|b_k|^{1/2})$ the region in which the nonlinearities are important will expand to occupy the whole flow, implying that the concept of a critical layer will eventually break down. Hence we turn to a numerical solution of the full equation (2.3) in order to study this process. The investigation will not be restricted to the long wave limit which has just been considered here for illustrative purposes.

CHAPTER 3. NUMERICAL FORMULATION

3.1 x-discretization

The periodicity in x is exploited by using Fourier series representations in x:

$$\Phi(x,y,t) \doteq \sum_{n=-N}^{N} \phi_n(y,t)\, e^{inx}$$

$$\varsigma(x,y,t) \doteq \sum_{n=-N}^{N} \varsigma_n(y,t)\, e^{inx}$$

Note that, because Φ and ς are real, $\phi_{-n}(y,t) = \phi_n^*(y,t)$ and $\varsigma_{-n}(y,t) = \varsigma_n^*(y,t)$ where * denotes complex conjugate. Using the orthogonality property of the e^{inx} equations (2.2) and (2.3) lead to

$$\frac{\partial \varsigma_n}{\partial t} + in\left\{\bar{u}\,\varsigma_n + \left(\beta - \frac{d^2\bar{u}}{dy^2}\right)\phi_n\right\} + \epsilon \sum_{l=-N+n}^{N} il\left\{\phi_l \frac{\partial \varsigma_{n-l}}{\partial y} - \varsigma_l \frac{\partial \phi_{n-l}}{\partial y}\right\}$$

$$= \nu\left(\frac{\partial^2 \varsigma_n}{\partial y^2} - \alpha^2 n^2 \varsigma_n\right) - \delta_0^n \frac{\nu}{\epsilon}\frac{d^3\bar{u}}{dy^3} \qquad (3.1)$$

and

$$\frac{\partial^2 \phi_n}{\partial y^2} - \alpha^2 n^2 \phi_n = \varsigma_n \,. \qquad (3.2)$$

Here δ_k^l is the Kronecker delta. The initial and forcing conditions become

$$\phi_n(y,0) = 0$$

$$\phi_n(y_m,t) = \delta_k^n \,.$$

At the southern boundary y_1 a radiation condition of the type presented

by Béland and Warn (1975) is applied. It allows only outward propagating energy (i.e., away from the source) and assumes that

(i) the boundary is far enough away from the critical layer for the flow to be linear and inviscid,

(ii) the initial wind profile $\bar{u}(y)$ is constant beyond this boundary, and

(iii) $\Phi(x, y, 0) = 0$ beyond this boundary.

In a form appropriate to this model it is, for steady waves with $\bar{u} < 0$:

$$\frac{d\phi_n}{dy} - \left(\alpha^2 n^2 - \frac{\beta}{\bar{u}}\right)^{1/2} \phi_n = 0$$

and for transient waves :

$$\frac{\partial \phi_n}{\partial y} - \alpha n . \phi_n = - \int_0^t \phi_n(y, \tau)\, W_n(t-\tau)\, d\tau$$

where $$W_n(\xi) = \frac{\beta}{2\alpha} e^{-in\left(\bar{u} - \frac{\beta}{2\alpha^2 n^2}\right)\xi} \left\{ J_1\left(\frac{\beta}{2\alpha^2 n} \xi\right) + i J_0\left(\frac{\beta}{2\alpha^2 n} \xi\right) \right\}.$$

3.2 t-discretization

Let $t = j \Delta t$ where Δt is the timestep interval and j is the timestep index. Define $\phi_n^j(y)$ and $\zeta_n^j(y)$ by

$$\phi_n(y,t) = \phi_n(y, j\Delta t) = \phi_n^j(y)$$

$$\zeta_n(y,t) = \zeta_n(y, j\Delta t) = \zeta_n^j(y).$$

A centered time scheme will be used and hence it will be necessary to lag the calculation of the viscous terms to ensure numerical

stability. Thus the time discretized versions of equations (3.1) and (3.2) are

$$\frac{\varsigma_n^{j+1}(y) - \varsigma_n^{j-1}(y)}{2\Delta t} = -in\left\{\bar{u}\,\varsigma_n^{j}(y) + \left(\beta - \frac{d^2\bar{u}}{dy^2}\right)\phi_n^{j}(y)\right\}$$

$$-\epsilon \sum_{\ell=-N+n}^{N} i\ell\left\{\phi_\ell^{j}(y)\frac{d\varsigma_{n-\ell}}{dy} - \varsigma_\ell^{j}(y)\frac{d\phi_{n-\ell}^{j}}{dy}\right\}$$

$$+\nu\left\{\frac{d^2\varsigma_n^{j-1}}{dy^2} - \alpha^2 n^2\,\varsigma_n^{j-1}(y)\right\} - \delta_0^n \frac{\nu}{\epsilon}\frac{d^3\bar{u}}{dy^3}$$

and $$\frac{d^2\phi_n^{j+1}}{dy^2} - \alpha^2 n^2\,\phi_n^{j+1}(y) = \varsigma_n^{j+1}(y). \qquad (3.3)$$

The northern boundary condition becomes

$$\phi_n^{j+1}(y_m) = \delta_k^n .$$

while the steady radiation condition at y_1 takes the form

$$\frac{d\phi_n^{j+1}}{dy}(y_1) - \left(\alpha^2 n^2 - \frac{\beta}{\bar{u}}\right)^{1/2}\phi_n^{j+1}(y_1) = 0.$$

Using a trapezoidal approximation for the integral in the transient radiation condition gives

$$\frac{d\phi_n^{j+1}}{dy}(y_1) - \left(\alpha n - i\,\frac{\beta\Delta t}{4a}\right)\phi_n^{j+1}(y_1) = -\Delta t\left\{\frac{\phi_n^{0}(y_1)\,W_n^{j+1}}{2} + \sum_{\ell=1}^{j}\phi_n^{\ell}(y_1)\,W_n^{(j+1)-\ell}\right\}$$

where $W_n^{\ell} = W_n(\ell\Delta t)$. By using asymptotic expansions of the Bessel functions it has been possible to derive an efficient approximation to the transient radiation condition. This approximation is presented in the appendix.

3.3 y-discretization

One of the most important features of this model is the use of finite elements in y. In the critical layer the scales of motion become very short and require high resolution for adequate simulation while in the rest of the domain the solution remains smooth. It is therefore desirable to use a numerical scheme which can easily and accurately incorporate variable resolution. One such scheme is provided by the finite element method.

To apply the method to the current problem it is necessary to know how to

(i) represent functions in terms of finite elements,

(ii) differentiate,

(iii) multiply, and

(iv) solve the diagnostic boundary value problem (equation 3.3).

A brief description of each of these procedures follows. For more detail on these and related applications of the finite element method see Staniforth and Daley (1977) and Staniforth and Mitchell (1977, 1978).

(i) To represent a function in terms of finite elements :

Suppose u(y) is a function defined on $y_1 \leq y \leq y_M$ and $\hat{u}(y)$ is the approximation to u(y). In the finite element method $\hat{u}(y)$ is written as a finite series

$$\hat{u}(y) = \sum_{m=1}^{M} u_m e^m(y)$$

where the $e^m(y)$ are piecewise defined polynomials which only interact locally, leading to sparse matrices whose structure can be exploited to produce efficient numerical schemes. Once the $e^m(y)$ are chosen, determining the coefficients u_m determines $\hat{u}(y)$. To find the M unknowns $u_1, \ldots, u_M$ it is necessary to impose M independent constraints. The accuracy of the scheme and complexity of the matrices depend on the degree of the polynomials chosen for the $e^m(y)$. We choose the $e^m(y)$ to be the "chapeau functions" depicted in figure 1 which lead to simple matrices (generally tri-diagonal) while providing high accuracy (fourth order over regions of uniform mesh length). Each chapeau function has the value 1 at its central mesh point, decays linearly to zero as the adjacent mesh points are approached, and remains zero beyond. Note that $e^m(y_k) = \delta_k^m$ (the Kronecker delta function). The u_m are determined by the "interpolatory constraints"

$$u(y_k) = \hat{u}(y_k) = \sum_{m=1}^{M} u_m e^m(y_k) = \sum_{m=1}^{M} u_m \delta_k^m = u_k .$$

Thus the approximation $\hat{u}(y)$ fits u(y) exactly at the mesh points y_m. It is an easy matter to show that for $y_k < y < y_{k+1}$ u(y) is a linear interpolation between mesh point values u_k and u_{k+1} as shown in figure 1.

(ii) To differentiate :

Assuming u(y) is a known function, the problem is to find $\hat{w}(y)$ approximating $w(y) = \frac{du}{dy}$. To do this, write

$$\hat{w}(y) = \sum_{m=1}^{M} w_m e^m(y), \qquad \hat{u}(y) = \sum_{m=1}^{M} u_m e^m(y)$$

where the u_m are as given in (i), and the w_m are M unknown coefficients. Substituting these gives

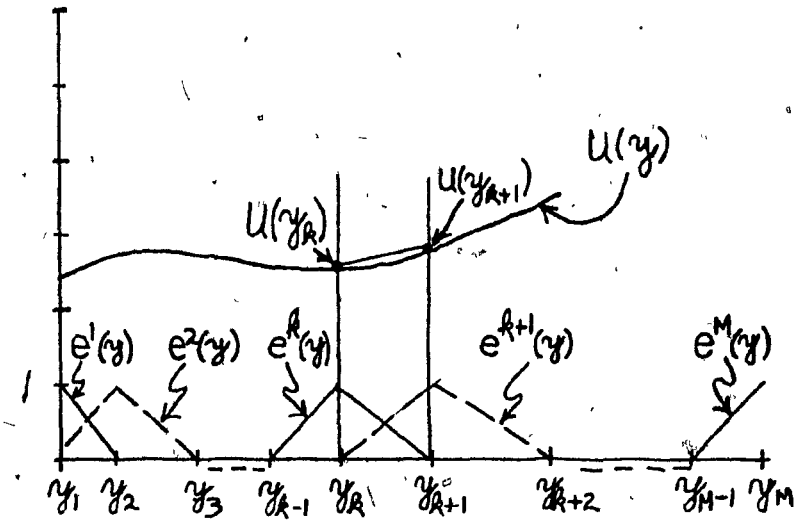

FIGURE 1

"CHAPEAU" BASIS FUNCTIONS

$$\hat{w}(y) - \frac{d\hat{u}}{dy} = E(y)$$

where E(y) is the error resulting from the approximations. The w_m can now be determined by imposing the Galerkin (or orthogonality) constraints

$$\int_{y_1}^{y_M} \left\{ \hat{w}(y) - \frac{d\hat{u}}{dy} \right\} e^k(y)\, dy = \int_{y_1}^{y_M} E(y)\, e^k(y) dy = 0 ,$$

that is $$\sum_{m=1}^{M} w_m \int_{y_1}^{y_M} e^m(y)\, e^k(y)\, dy - \sum_{m=1}^{M} u_m \int_{y_1}^{y_M} \frac{de^m}{dy} e^k(y)\, dy = 0$$

or $$\sum_{m=1}^{M} P^{km} w_m = \sum_{m=1}^{M} P_y^{km} u_m \qquad (3.4)$$

where $P^{km} = \int_{y_1}^{y_M} e^k(y)\, e^m(y)\, dy$ and $P_y^{km} = \int_{y_1}^{y_M} e^k(y)\, \frac{de^m}{dy}\, dy$.

Since k assumes the values $1, \ldots, M$, (3.4) is a system of M equations for the M unknowns w_m, and can conveniently be written in matrix form. The fact that the $e^m(y)$ are zero for $y \geq y_{m+1}$ or $y \leq y_{m-1}$ means that $P^{km} = P_y^{km} = 0$ unless $m = k-1, k,$ or $k+1$. The resulting matrices are tri-diagonal and this fact can be exploited to produce efficient solution schemes (Gaussian elimination for the tri-diagonal problem, see Ahlberg et al., 1967, p. 14). With h_k representing $y_{k+1} - y_k$ the matrix form of $w(y) = du/dy$ is

$$\begin{bmatrix} \frac{h_1}{3} & \frac{h_1}{6} & & & & \\ \frac{h_1}{6} & \frac{h_1+h_2}{3} & \frac{h_2}{6} & & 0 & \\ & \ddots & \ddots & \ddots & & \\ & & \frac{h_{k-1}}{6} & \frac{h_{k-1}+h_k}{3} & \frac{h_k}{6} & \\ & 0 & & \ddots & \ddots & \frac{h_{M-1}}{6} \\ & & & & \frac{h_{M-1}}{6} & \frac{h_{M-1}}{3} \end{bmatrix} \begin{bmatrix} w_1 \\ w_2 \\ \vdots \\ w_k \\ \vdots \\ w_{M-1} \\ w_M \end{bmatrix} = \begin{bmatrix} -\frac{1}{2} & \frac{1}{2} & & & & \\ -\frac{1}{2} & 0 & \frac{1}{2} & & 0 & \\ & \ddots & \ddots & \ddots & & \\ & & -\frac{1}{2} & 0 & \frac{1}{2} & \\ & 0 & & \ddots & \ddots & \frac{1}{2} \\ & & & & -\frac{1}{2} & \frac{1}{2} \end{bmatrix} \begin{bmatrix} u_1 \\ u_2 \\ \vdots \\ u_k \\ \vdots \\ u_{M-1} \\ u_M \end{bmatrix}.$$

(iii) To multiply :

Assuming u(y) and v(y) are known, we want to find $\hat{w}(y)$ approximating $w(y) = u(y)\, v(y)$. Write

$\hat{w}(y) = \sum_{m=1}^{M} w_m e^m(y)$, $\hat{u}(y) = \sum_{m=1}^{M} u_m e^m(y)$, and $\hat{v}(y) = \sum_{m=1}^{M} v_m e^m(y)$

where the u_m and v_m are as given in (i) and we want to determine the M unknown coefficients w_m. Proceeding as before,

$$\int_{y_1}^{y_M} \{ \hat{w}(y) - \hat{u}(y)\, \hat{v}(y) \}\, e^k(y)\, dy = 0$$

leads to $$\sum_{m=1}^{M} P^{km} w_m = \sum_{l=1}^{M} \sum_{m=1}^{M} u_l\, Q^{klm} v_m$$

where the P^{km} are the same as in (3.4) and

$$Q^{klm} = \int_{y_1}^{y_M} e^k(y)\, e^l(y)\, e^m(y)\, dy.$$

Evaluating the integrals gives

$$Q^{111} = \frac{h_1}{4} \qquad Q^{112} = Q^{121} = Q^{122} = \frac{h_1}{12}$$

$$Q^{MMM} = \frac{h_{M-1}}{4} \qquad Q^{M(M-1)M} = Q^{MM(M-1)} = Q^{M(M-1)(M-1)} = \frac{h_{M-1}}{12}$$

while for $k = 2, \ldots, M-1$ Q^{klm} is given by

m \ l	k-1	k	k+1
k-1	$\frac{h_{k-1}}{12}$	$\frac{h_{k-1}}{12}$	0
k	$\frac{h_{k-1}}{12}$	$\frac{h_{k-1}+h_k}{4}$	$\frac{h_k}{12}$
k+1	0	$\frac{h_k}{12}$	$\frac{h_k}{12}$

with $Q^{klm} = 0$ otherwise.

(iv) To solve the diagnostic boundary value problem :

$$\frac{d^2\phi_n^{s+1}}{dy^2} - \alpha^2 n^2 \phi_n^{s+1}(y) = \varsigma_n^{s+1}(y) . \qquad (3.3)$$

The forcing boundary condition is imposed at $y = y_M$ and can be written as

$$\phi_n^{s+1}(y_M) = a + ib$$

for appropriate values of the real constants a and b.

The radiation boundary condition is imposed at y_1 and can be written as

$$\frac{d\phi_n^{s+1}}{dy}(y_1) - (n - i\xi)\,\phi_n(y_1) = c + id$$

for appropriate values of the real constants η, ξ, c, and d.

Writing

$$\phi_n^{s+1}(y) = u(y) + i\,v(y)$$

$$\varsigma_n^{s+1}(y) = r(y) + i\,s(y)$$

and $\lambda = \alpha n$ allows separation into a pair of real boundary value problems

(A) $$\frac{d^2u}{dy^2} - \lambda^2 u(y) = r(y)$$

with boundary conditions $u(y_M) = a$,

and $$\frac{du}{dy}(y_1) - \eta\, u(y_1) - \xi\, v(y_1) = c ,$$

(B) $$\frac{d^2v}{dy^2} - \lambda^2 v(y) = s(y)$$

with boundary conditions $v(y_M) = b$,

and $$\frac{dv}{dy}(y_1) - \eta\, v(y_1) + \xi\, u(y_1) = d .$$

Note that these problems are coupled through the boundary conditions at y_1.

Consider problem (A) :

$$\frac{d^2u}{dy^2} - \lambda^2 u(y) = r(y) .$$

Multiplying be $e^k(y)$ and integrating gives

$$\int_{y_1}^{y_M} \frac{d^2u}{dy^2} e^k(y)\,dy - \lambda^2 \int_{y_1}^{y_M} u(y)\, e^k(y)\,dy = \int_{y_1}^{y_M} r(y)\, e^k(y)\,dy .$$

Doing an integration by parts on the first term,

$$\int_{y_1}^{y_M} \frac{d^2u}{dy^2} e^k(y)\,dy = \delta_M^k \frac{du}{dy}(y_M) - \delta_1^k \frac{du}{dy}(y_1) - \int_{y_1}^{y_M} \frac{du}{dy}\frac{de^k}{dy}\,dy .$$

The southern boundary condition (at y_1) can be written as

$$\frac{du}{dy}(y_1) = \eta\, u(y_1) + \xi v(y_1) + C$$

and combining these results gives

$$\delta_M^k \frac{du}{dy}(y_M) - \delta_1^k \{\eta u(y_1) + \xi v(y_1) + C\} - \int_{y_1}^{y_M} \frac{du}{dy}\frac{de^k}{dy}\,dy$$

$$-\lambda^2 \int_{y_1}^{y_M} u(y)\, e^k(y)\,dy = \int_{y_1}^{y_M} r(y)\, e^k(y)\,dy . \qquad (3.5)$$

The finite element schemes presented up to this point have been accurate to fourth order in h_k over regions with constant h_k and to second order over regions of varying h_k (see Cullen, 1976, and section 7.2 of Strang and Fix for a discussion of errors in the finite element method). If we use

$$u(y) \doteq \hat{u}(y) = \sum_{m=1}^{M} u_m e^m(y) , \quad r(y) \doteq \hat{r}(y) = \sum_{m=1}^{M} i_m e^m(y)$$

in equation (3.5) it is found that the solutions are only second order accurate over regions of constant h_k. The desired fourth order accuracy can be maintained by introducing parabolic approximations $\hat{u}(y)$, $\hat{r}(y)$ for functions $u(y)$ and $r(y)$ in equation (3.5) :

$$\hat{u}(y) = u_{k-1}\left(\frac{y-y_k}{h_{k-1}}\right)^2 + u_k\left\{1-\left(\frac{y-y_k}{h_{k-1}}\right)^2\right\} \quad y_{k-1}\le y\le y_k$$

$$= u_k\left\{1-\left(\frac{y-y_k}{h_k}\right)^2\right\} + u_{k+1}\left(\frac{y-y_k}{h_k}\right)^2 \quad y_k\le y\le y_{k+1}$$

$$= 0 \qquad \text{otherwise,}$$

with a similar scheme for $\hat{r}(y)$. This is the one-dimensional equivalent of the method given in appendix B of Staniforth and Mitchell (1978). Evaluating the resulting integrals, equation (3.5) becomes,

for k = 1 :

$$-\left(\frac{1}{h_1}+\lambda^2\frac{5}{12}h_1+\eta\right)u_1+\left(\frac{1}{h_1}-\lambda^2\frac{h_1}{12}\right)u_2-\xi v_1=\frac{5}{12}r_1+\frac{h_1}{12}r_2+c$$

for k = 2, ..., M-1 :

$$\left(\frac{1}{h_{k-1}}-\lambda^2\frac{h_{k-1}}{12}\right)u_{k-1}-\left\{\frac{1}{h_{k-1}}+\frac{1}{h_k}+\lambda^2\frac{5}{12}(h_{k-1}+h_k)\right\}u_k$$

$$+\left(\frac{1}{h_k}-\lambda^2\frac{h_k}{12}\right)u_{k+1}=\frac{h_{k-1}}{12}r_{k-1}+\frac{5}{12}(h_{k-1}+h_k)r_k+\frac{h_k}{12}r_{k+1}\,.$$

As an M^{th} equation use the northern boundary condition $u(y_M) = u_M = q$.

A similar procedure for problem (B) gives another set of M equations, so we have a total of 2M equations for the 2M unknown coefficients $u_1, \ldots, u_M$, $v_1, \ldots, v_M$ and the problem is solved. It can be expressed as the following almost tri-diagonal matrix problem for which an efficient solution algorithm exists (Gaussian elimination for the almost tri-diagonal problem, see Ahlberg et al., 1967, p. 15).

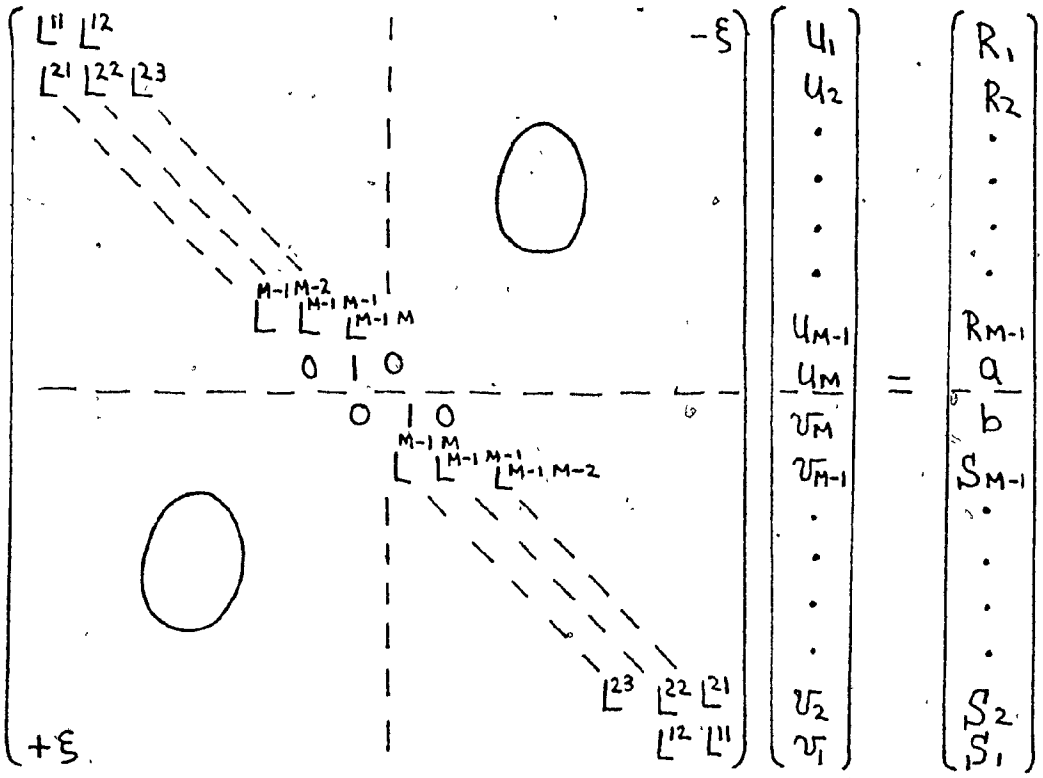

where

$$L^{11} = -\left(\frac{1}{h_1} + \lambda^2 \frac{5}{12} h_1 + \gamma\right) \qquad L^{12} = \frac{1}{h_1} - \lambda^2 \frac{h_1}{12}$$

$$\left.\begin{aligned} L^{k\,k-1} &= \frac{1}{h_{k-1}} - \lambda^2 \frac{h_{k-1}}{12} \\ L^{k\,k} &= -\left\{\frac{1}{h_{k-1}} + \frac{1}{h_k} + \lambda^2 \frac{5}{12}(h_{k-1} + h_k)\right\} \\ L^{k\,k+1} &= \frac{1}{h_k} - \lambda^2 \frac{h_k}{12} \end{aligned}\right\} \quad k = 2, \ldots, M-1$$

$$R_1 = \frac{5}{12} r_1 + \frac{h_1}{12} r_2 + c \qquad R_k = \frac{h_{k-1}}{12} r_{k-1} + \frac{5}{12}(h_{k-1} + h_k) r_k + \frac{h_k}{12} r_{k+1}$$

$$S_1 = \frac{5}{12} s_1 + \frac{h_1}{12} s_2 + d. \qquad S_k = \frac{h_{k-1}}{12} s_{k-1} + \frac{5}{12}(h_{k-1} + h_k) s_k + \frac{h_k}{12} s_{k+1}.$$

This completes the numerical formulation of the problem.

CHAPTER 4. EXPERIMENTS

In this chapter we will present details of two sets of experiments using the numerical model described in the previous chapter. The first set deals with the dependence of the logarithmic phase shift on the relative strengths of viscosity and nonlinearity, while the second set investigates the potential nonlinear critical layer resonance mechanism for Rossby waves which was suggested in the latter part of chapter 2.

4.1 Selection of parameters

Among the quantities to be specified are the initial wind profile $\bar{u}(y)$, the non-dimensional time step interval Δt, NW the number of waves in the x-direction, k the wavenumber of the forced wave, $h(y)$ the profile of mesh lengths in the y-direction, and the values of the non-dimensional parameters α, β, ϵ, ν.

The initial wind profile of figure 2 was used for all the experiments. Throughout most of the domain $\bar{u}$ is linear with a zero at $y = 0$. For $y < -\frac{1}{3}$ the profile is a hyperbolic tangent function which asymptotes to a constant value (-1). $\bar{u}$ is therefore in the class of profiles assumed in the derivation of the radiation condition. The value of β was always chosen to ensure that $\beta - \frac{d^2\bar{u}}{dy^2} > 0$ everywhere in the domain, thus excluding the possibility of barotropic instabilities.

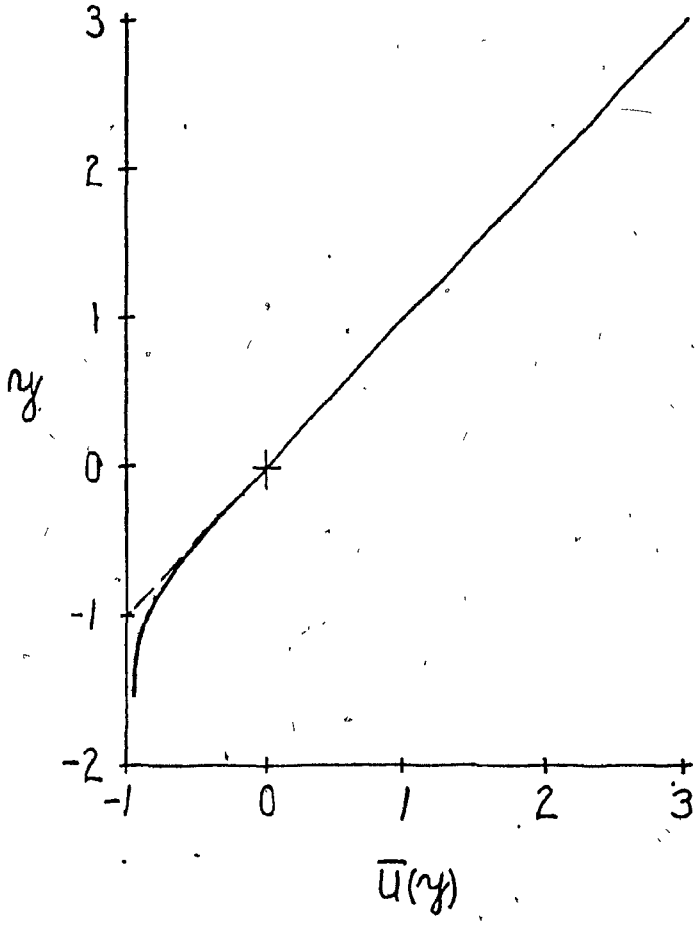

FIGURE 2

INITIAL WIND PROFILE

The mesh length profiles are shown in figure 3. In the majority of runs profile (A) was used. Here the mesh length has a constant value of .02 in the vicinity of the critical layer and increases to .1 and .2 to the north and south. Tests confirmed that varying the resolution in this way did not introduce significant error. It is found that the amplitude of the solution decreases rapidly to the south of the critical layer and this probably accounts for the fact that a lower resolution can be tolerated in that region. Using profile (A) it is possible to cover $-1.5 \leq y \leq 2.5$ with slightly less than 100 mesh points, while using a uniform resolution of .02 would require 200 points. This results in a considerable saving while retaining the desired accuracy in the critical layer. In profile (B) the region of uniform high resolution is extended to the northern boundary. This was used in a few of the resonance experiments to ensure that the expanding critical layer would be adequately resolved and also to facilitate undistorted contouring of the output fields.

Invariably α was chosen to be .4, k was 1, while the number of waves in the x-direction (NW) varied from 1 for the linearized runs up to 20 in the most nonlinear case. Δt was generally .035 which is somewhat less than the limit required for computational stability. β was always in the range 1.2 to 2.0, with the central value of 1.6 corresponding to a choice of length scale L = 1000 km. and velocity scale U_s = 10 m/s at a latitude of 45 degrees. In the nonlinear runs the transient radiation condition was imposed on wavenumbers 1-3 while the steady condition was used for higher wavenumbers. The forcing at the northern boundary was switched on linearly over the first 100 timesteps.

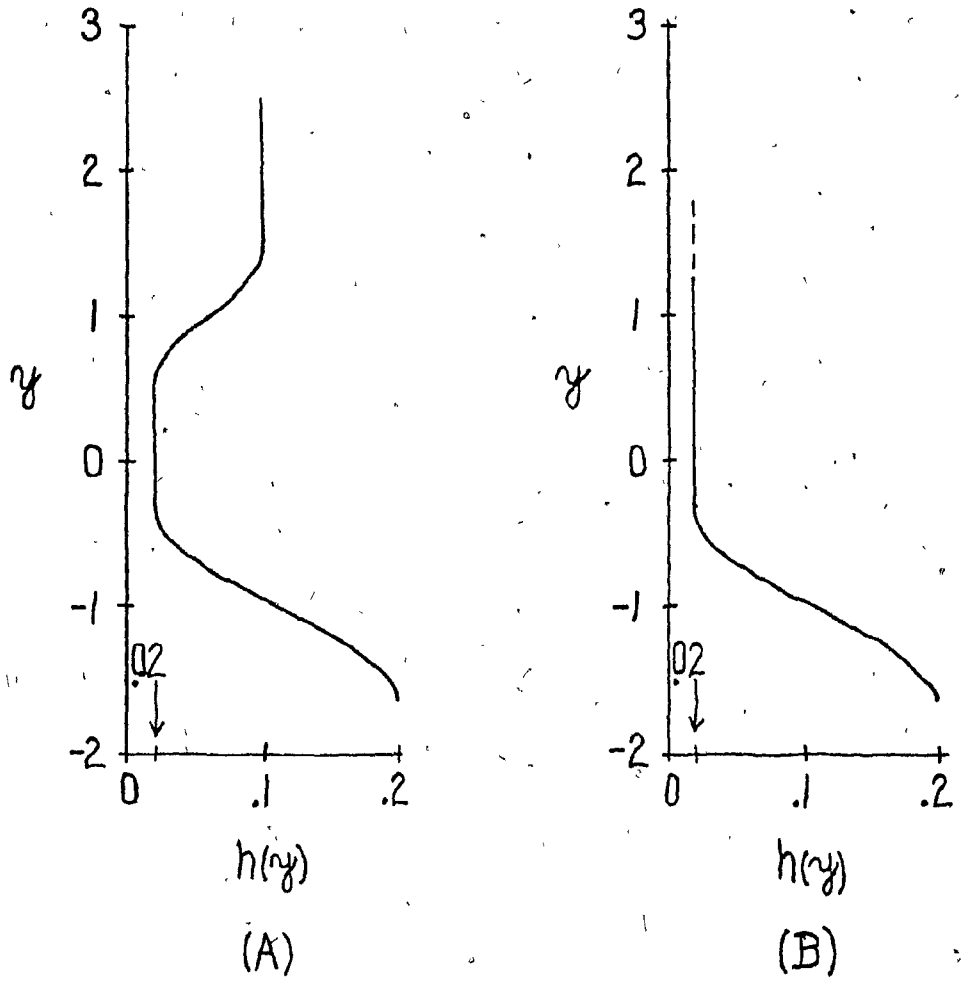

FIGURE 3

MESH LENGTH PROFILES

Significant parameters for the experiments to be described here are ν and ϵ, or the combination $\lambda = \nu/\epsilon^{3/2}$ which gives a measure of the relative importance of the viscous and nonlinear effects. The values of ν and ϵ vary considerably and will be indicated in the more detailed description of the experiments.

4.2 The logarithmic phase shift

We shall now describe the experiments performed to investigate the dependence of the logarithmic phase shift on the relative strengths of viscosity and nonlinearity. Recall that the analysis of the steady state problem suggested that it should be possible to resonantly excite a Rossby wave provided that the logarithmic phase shift tends to zero.

For our wind profile the expression (2.9) for the real part of θ becomes

$$\theta_R = \frac{[R]}{2\beta k |b_k|^2}$$

where $[R]$ denotes the jump in the Reynolds stress across the critical layer.

Haberman (1972) analysed the dependence of θ_R on ν and ϵ for the steady problem and obtained θ_R as a function of λ_c which, for the present case, is given by

$$\lambda_c = \frac{\lambda}{k(2|b_k|)^{3/2}} .$$

For the steady problem it can be shown that the Reynolds stress

$$R = \frac{1}{2\pi} \int_0^{2\pi} \Phi_x \Phi_y \, dx$$

is constant outside the critical layer, being zero below the layer for the wind profile and southern boundary condition used here. Therefore $[R]$ is given by R evaluated at any point above the critical layer.

In our model, however, these quantities will be functions of time. Warn and Warn (1978) show that in the time dependent non-linear problem a first approximation to the coefficient of the forced wave $\phi_k(y,t)$ is given by $A_k(\tau)\,\phi_{a,k}(y) + B_k(\tau)\,\phi_{b,k}(y)$ where $\tau = \epsilon^{1/2} t$ is a slow time scale. That is, the role of b_k in the steady problem is played by $B_k(\tau) \doteq \phi_k(0,t)$ in the time dependent problem and accordingly we define

$$\theta_R(t) = \frac{[R_k(t)]}{2\beta k \, |\phi_k(0,t)|^2}$$

$$\lambda_c(t) = \frac{\lambda}{2^{3/2} k \, |\phi_k(0,t)|^{3/2}}$$

where $[R_k(t)]$ is the jump across the critical layer in the Reynolds stress of the forced wave. The Reynolds stress can be expressed as $R_k = -2\,\mathrm{Im}\left(\phi_k \frac{\partial \phi_k^*}{\partial y}\right)$ with Im( ) denoting the imaginary part. In the numerical integrations it was found that, at any given time, R_k showed some dependence on y, decaying quickly to zero below the critical layer and varying slightly about an easily identifiable mean value above the layer. Because of this behavior it was decided to take $[R_k(t)]$ as the y-average of the values of R_k above the critical layer at time t.

In figure 4 the evolution of $\theta_R(t)$ is presented for six different runs. Haberman's analysis neglected the term corresponding to $\frac{\nu}{\epsilon}\frac{d^3\bar{u}}{dy^3}$ in equation (2.3), and this term was also removed from our model for runs 1, 2, 3, and 4. The values of the relevant parameters are given in the following table :

TABLE 1 : Logarithmic phase shift runs

RUN	λ	ϵ	ν	NW	β	y_M
1	∞	——	2.16×10^{-4}	1	1.60	2.24
2	4	.0016	2.56×10^{-4}	4	1.60	2.24
3	2	.0016	1.28×10^{-4}	4	1.60	2.24
4	1	.0036	2.16×10^{-4}	4	1.60	2.24
5	.5	.0064	2.56×10^{-4}	8	1.43	2.24
6	.5	.0064	2.56×10^{-4}	8	1.60	1.54

Runs 1 through 4 became steady by $t \sim 100$, while runs 5 and 6 showed slight oscillation in time and were integrated to $t \sim 200$ in order to have at least one complete oscillation -- the steady state value then being taken as the mean over the oscillation. The steady values of θ_R and the corresponding values of λ_c are plotted as the dots (numbered according to run) in figure 5. The solid line is the curve presented by Haberman (his figure I) while the crosses mark the points recently reported by Béland (1978, his figure 10). The three sets of results show good qualitative agreement, despite the fact that Haberman neglected certain wave interactions (those not involving the primary wave) and it appears from recent work that these are important (Brown and Stewartson, 1978; Stewartson,

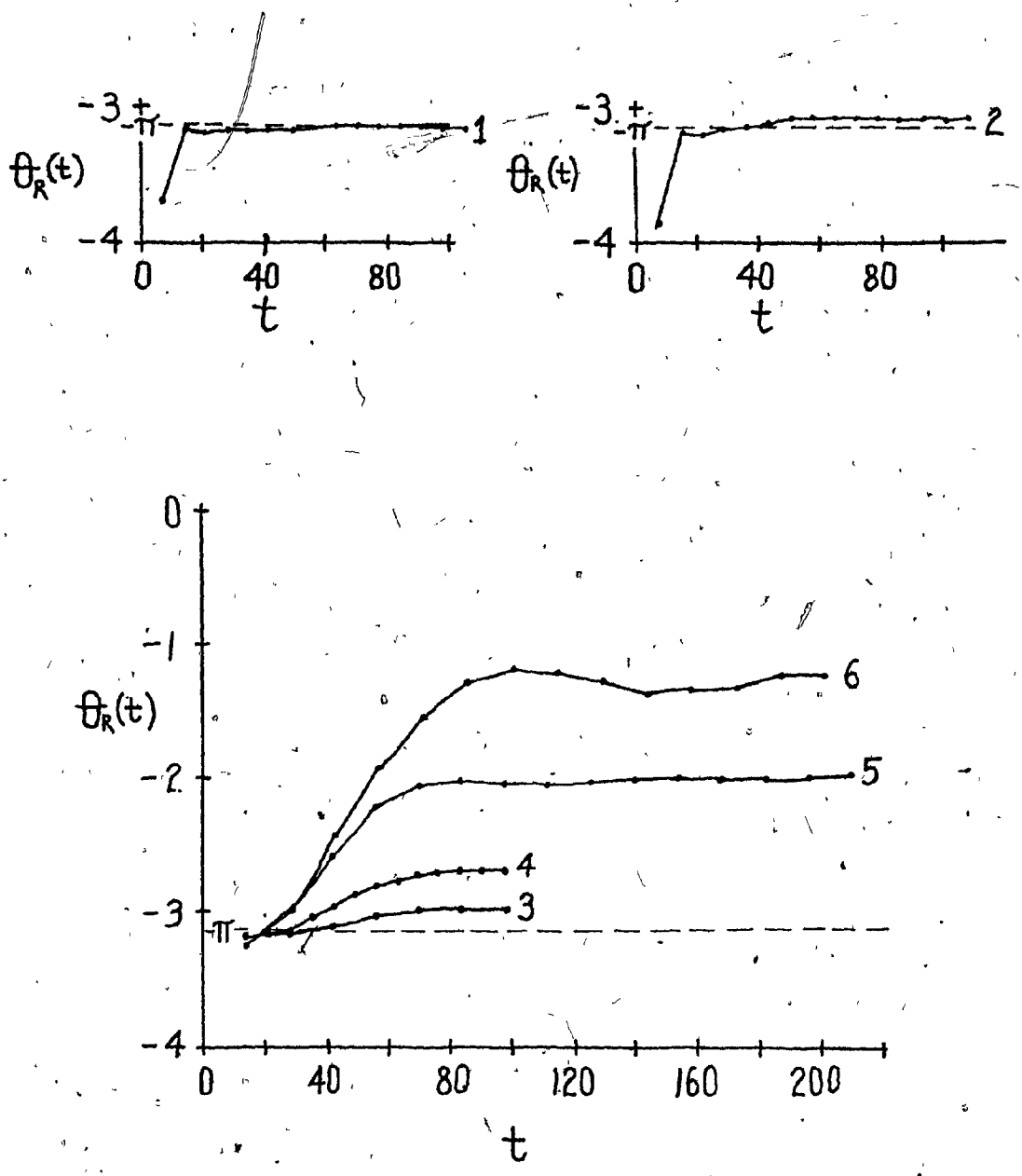

FIGURE 4

EVOLUTION OF $\theta_R(t)$. CURVES ARE NUMBERED ACCORDING TO RUNS GIVEN IN TABLE 1, PAGE 31.

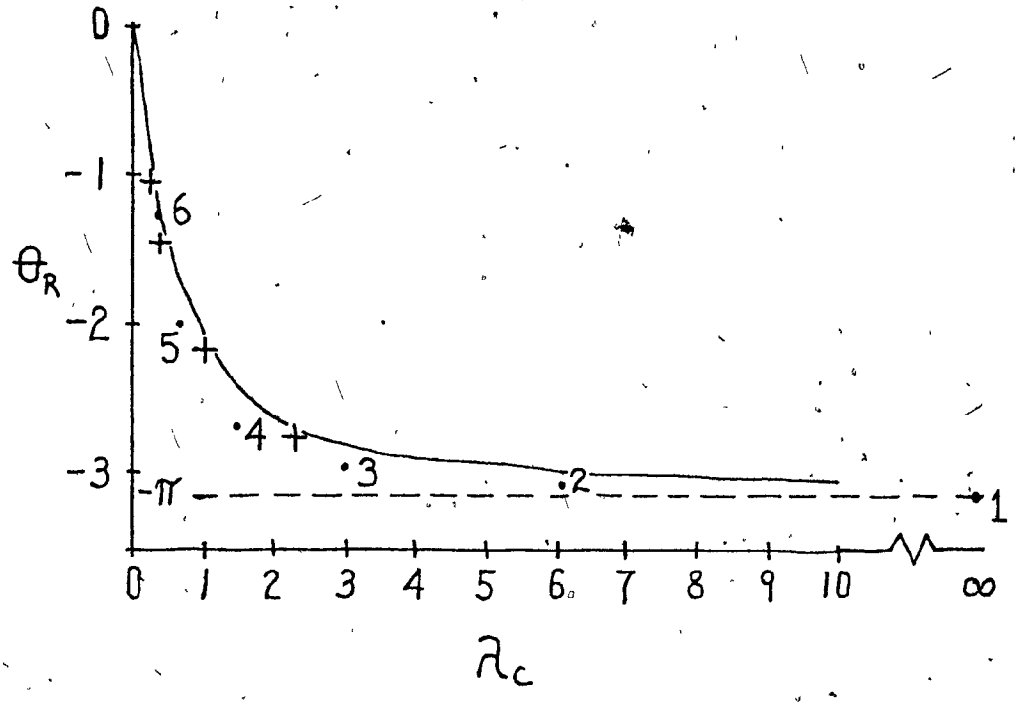

FIGURE 5

θ_R VERSUS λ_c. SOLID LINE IS HABERMAN'S CURVE (1972, FIG. 1). DOTS (NUMBERED ACCORDING TO RUN) GIVE STEADY STATE VALUES FOR CURVES IN FIG. 4. CROSSES MARK BÉLAND'S POINTS (1978, FIG. 10).

1978; Warn and Warn, 1978). If all interactions are included it seems that θ may also depend on the geometry of the flow (in addition to λ_c) and have an imaginary part. As will be shown in the next section, the complex nature of θ may be of particular relevance to the Rossby wave resonance mechanism.

4.3 Resonance experiments

Equation (2.11) shows that, in the long wave limit for a flow with a linear mean wind profile, the linearized steady state solution is proportional to $h_k = \phi_k(0)$. This suggests taking $\phi_k(0,t)$ as a measure of the response in the time dependent nonlinear problem, so we define the normalized response

$$r = \left| \frac{\phi_k(0,t)}{\phi_{kv}(0)} \right| \qquad (4.1)$$

where $\phi_{kv}(0)$ is the steady state value for a corresponding linearized run -- the linearization yielding viscosity as the controlling mechanism in the critical layer.

Our analysis for steady long waves indicated that by changing βy_m it might be possible to excite a free wave if nonlinearities dominate the critical layer. Experiments were performed to test this hypothesis. For the first group of resonance experiments λ had the value .5 (ϵ = .0064, $\nu = 2.56 \times 10^{-4}$), and NW was 8. Only β and y_m changed from run to run as given in the following table :

TABLE 2 : Resonance runs

RUN	β	y_M	βy_M
1	1.561	2.243	3.50
2	1.910	1.256	2.40
3	1.831	1.256	2.30
4	1.791	1.256	2.25
5	1.751	1.256	2.20
6	1.671	1.256	2.10
7	1.592	1.256	2.00
8	1.512	1.256	1.90
9	1.433	1.256	1.80
10	1.353	1.256	1.70

Figure 6 consists of curves, numbered according to run, giving the evolution of the normalized response for the different values of βy_M. Figure 6(A) gives the curves as βy_M decreases from a value of 3.50 to a value of 2.20, while figure 6(B) shows the curves as βy_M continues to decrease beyond 2.20 to reach a value of 1.70 in curve 10. The abscissa chosen for these curves is $\tau = \epsilon^{1/2} t$, the time scale of the nonlinearities (Warn and Warn, 1976). These curves confirm the hypothesis that a large amplitude response can be produced with the correct geometry and a nonlinear critical layer. Run 1 is definitely non-resonant -- during the whole integration the response stays within 5 per cent of its initial value. However, as βy_M decreases it is possible to produce larger and larger responses, with the near resonant runs 4 and 5 giving sevenfold amplifications by the ends of the integrations. Notice

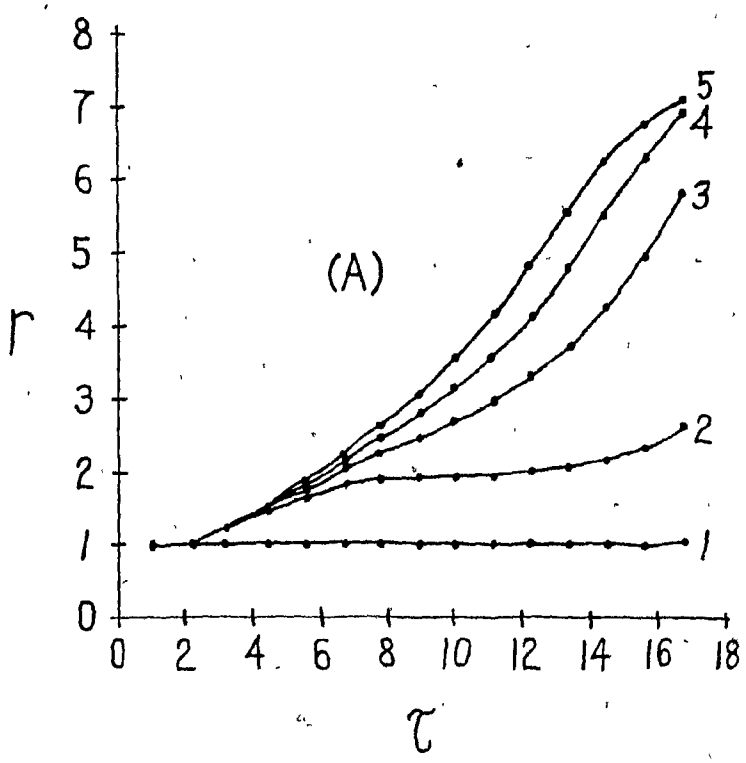

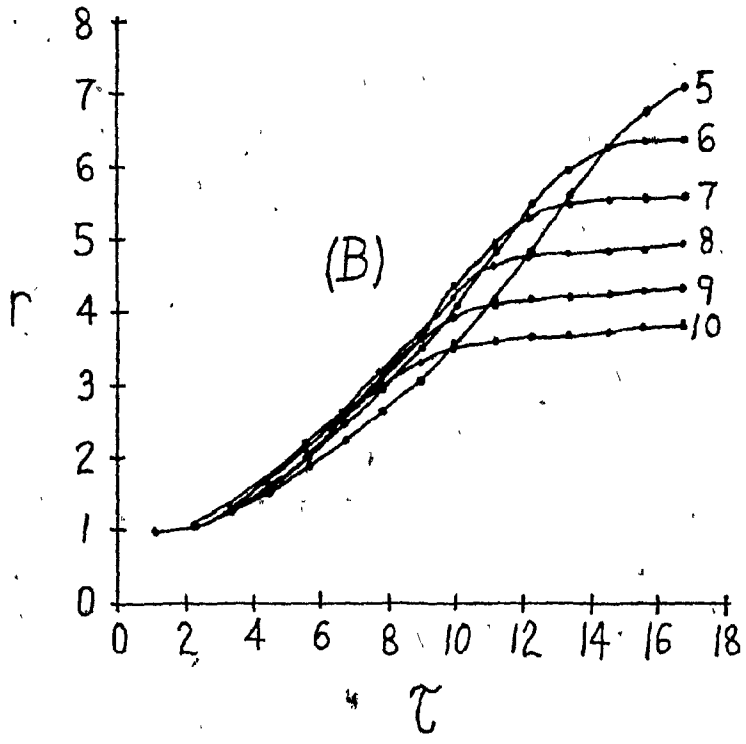

FIGURE 6

EVOLUTION OF RESPONSE. CURVES ARE NUMBERED BY RUN AS GIVEN IN TABLE 2, PAGE 35.

that, with the exception of run 1, none of the curves in figure 6(A) indicates that a steady state has been reached. As βy_M continues to decrease beyond its "resonant" value of 2.25 or 2.20, smaller and smaller responses are obtained at the end of the integrations as shown by figure 6(B). These curves also reveal a somewhat unexpected feature -- curves 6 through 10 cross curve 5 during the integration; that is, the run which eventually has the largest response in this set is initially the slowest growing. Efforts to explain this behavior led to a closer examination of the role of the logarithmic phase shift in the resonance mechanism.

For the steady, linear, inviscid problem the forcing boundary condition $\phi_k(y_m) = 1$ gives

$$a_k^+ \phi_{a,k}(y_m) + b_k \phi_{b,k}(y_m) = 1.$$

The decaying nature of the solution as $y \to -\infty$ requires $a_k^- = g\, b_k$ where g is a real constant. Combining these with the definition of Θ (equation 2.8) leads to

$$b_k = \frac{1}{c(\mu + i\theta)}$$

where for the wind profile used here

$$c = \beta\, \phi_{a,k}(y_m) \quad , \quad \mu = \frac{\phi_{b,k}(y_m) + g\, \phi_{a,k}(y_m)}{\beta\, \phi_{b,k}(y_m)} .$$

Replacing b_k by $\phi_k(0,t)$ again yields the time dependent analogue

$$\phi_k(0,t) = \frac{1}{c\{\mu + i\,\theta(t)\}} . \qquad (4.2)$$

Substituting into equation (4.1), taking $\Theta(t) = \Theta_R(t) + i\,\Theta_I(t)$, and

using the fact that $\theta = -\pi$ in the linearized case gives

$$r^2 = \frac{\mu^2 + \pi^2}{\{\mu - \theta_I(t)\}^2 + \{\theta_R(t)\}^2} \quad . \tag{4.3}$$

This equation shows that the response will be large if $\theta_I(t)$ approaches μ as $\theta_R(t)$ approaches zero. Separating equation (4.2) into real and imaginary parts leads to

$$\theta_I(t) = \mu + \theta_R(t) \frac{Re\{\phi_R(0,t)\}}{Im\{\phi_R(0,t)\}}$$

where $$\phi_R(0,t) = Re\{\phi_R(0,t)\} + i\, Im\{\phi_R(0,t)\} \quad .$$

$\theta_I(t)$ can be calculated using this equation, since μ can be found from a linear run and $\theta_R(t)$ can be calculated as described in section 4.2.

Using this method the values of θ_I were calculated for runs 2, 5, and 7 of figure 6. The evolutions of θ_R and θ_I are given in figure 7, where the horizontal lines in the lower frame give the corresponding values of μ. Notice that there is very little difference in the evolution of θ_R for the three runs, particularly up to $\tau = 10$, indicating that the response r is largely controlled by θ_I. Runs 5 and 7 show very similar evolutions of θ_I, but have significantly different values of μ. It is $\mu - \theta_I$ which appears in equation (4.3) and this quantity goes to zero at $\tau \doteq 9.5$ for run 7 but doesn't vanish until $\tau = 14$ for run 5. Thus it is $\mu - \theta_I$ which explains the fact that the response for run 7 initially grows faster and exceeds the response for run 5 by the greatest amount at $\tau \doteq 9.5$. However,

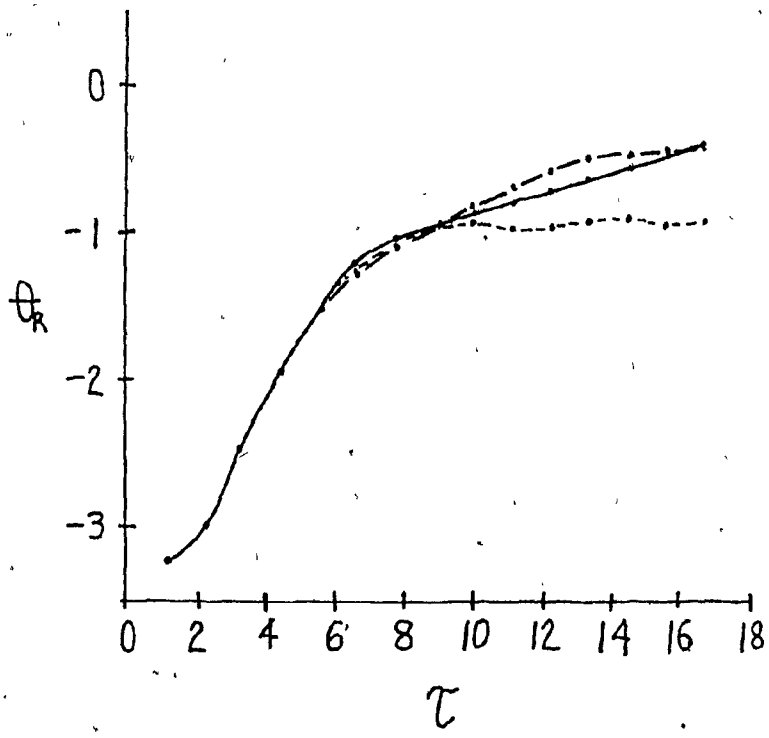

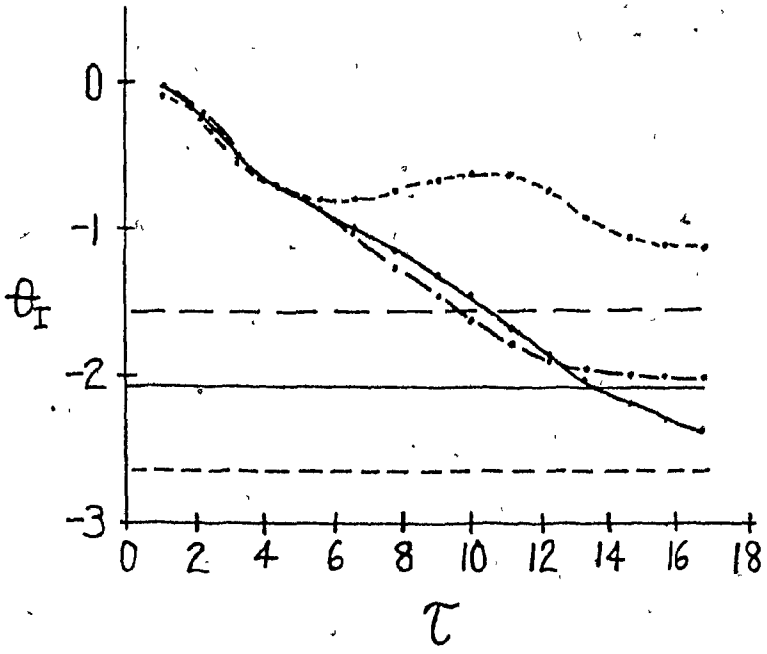

FIGURE 7

EVOLUTION OF θ FOR RUNS 2---, 5——, 7—— OF FIG. 6. HORIZONTAL LINES GIVE CORRESPONDING μ VALUES.

run 5 has the largest response eventually because $\mu - \theta_I$ and θ_R are simultaneously small towards the end of the run. On the other hand, $\mu - \theta_I$ remains large for run 2 throughout the entire integration and hence its response stays relatively small.

Figure 8 presents the evolution of the normalized response for two additional runs. In curve 1 the integration time for one of the resonant runs (run 4 of figure 6) was extended to see if the response would continue to grow rapidly or settle down. The number of waves, NW, was increased to 10 and resolution profile (B) of figure 3 was used. As can be seen in the figure, the response attains a value near 8 by the end of this run. To investigate the effect of larger nonlinearities a run was performed with $\lambda = .1$ ($\epsilon = .01$, $\nu = 10^{-4}$), $y_M = 2.20$, and NW = 20. The response is given in curve 2 of figure 8. The integration was carried out to $\tau \doteq 8.5$, by which time it was evident that more than 20 waves would be required to proceed further. A comparison of curves 1 (for which $\lambda = .5$) and 2 ($\lambda = .1$) shows that the growth of a large response is faster when the nonlinearities are more dominant. Further reduction in λ was attempted, but it was found that much higher resolution would be required. It would be desirable to implement a more efficient numerical scheme (e.g., the fast fourier transform) before pursuing this issue.

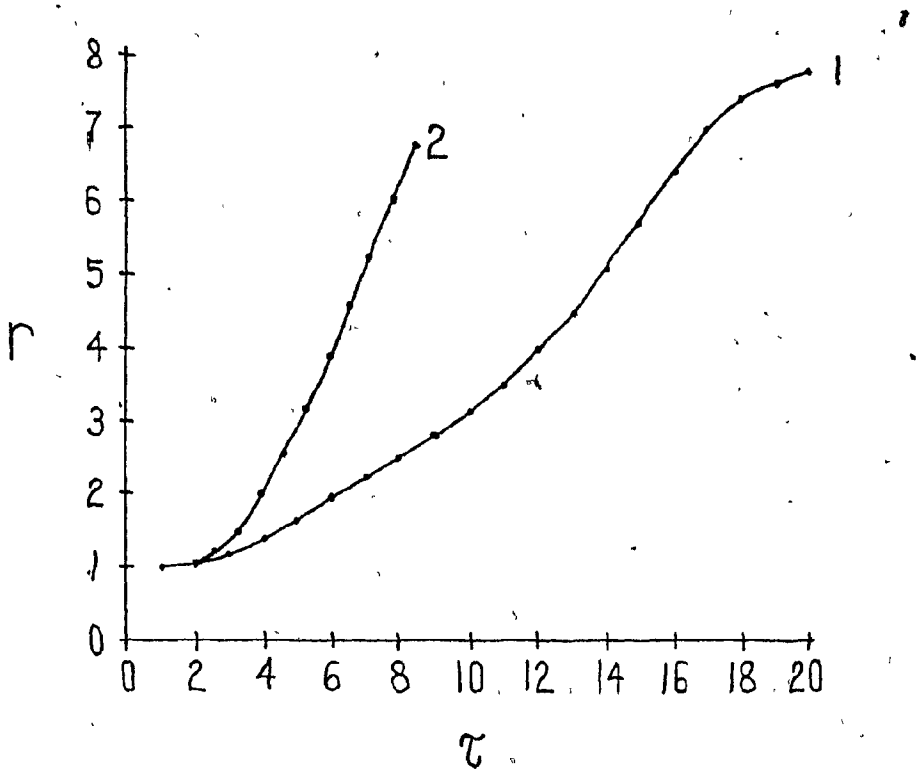

FIGURE 8

EVOLUTION OF RESPONSE.
CURVE 1: EXTENSION OF RUN 4 TABLE 2, PAGE 35
CURVE 2: RUN WITH λ REDUCED TO .1, $\beta\gamma_M = 2.20$

Figures 9 and 10 show the evolution of the total streamfunction and absolute vorticity patterns, respectively, for a resonant case (curve 1 of figure 8). Resolution profile (B) of figure 3 was used and y covers the range -.6 to +.9 in these patterns. The streamfunction field shows the "cat's eye" structure which is characteristic of flows in the vicinity of critical layers, and the associated absolute vorticity field exhibits the typical "rolling up" and development of intense gradients beginning near the edges of the cat's eye. Notice that, as suggested at the end of chapter 2, the critical layer spreads out as the response grows. The width of the critical layer can be taken as the width of the region containing closed streamfunction contours. This region is fairly narrow in the early stages as shown by figure 9(A) and in a nonresonant case (e.g., curve 1 or 2 of figure 6) the critical layer would not become much wider than this. However, the layer expands considerably in this resonant case to occupy a large portion of the total flow by the end of the run, as shown in figure 9(E).

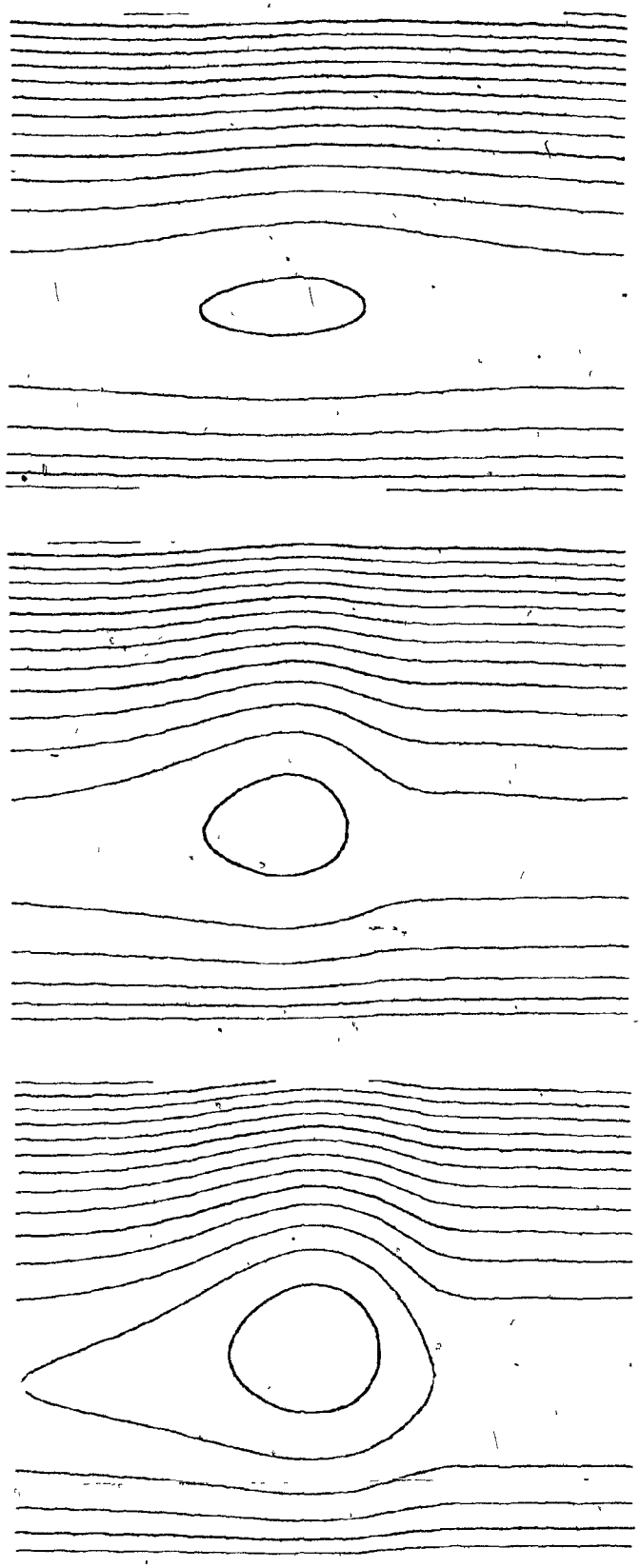

FIGURE 9

Total streamfunction for curve 1 of figure 8

(D)

$\tau = 16$

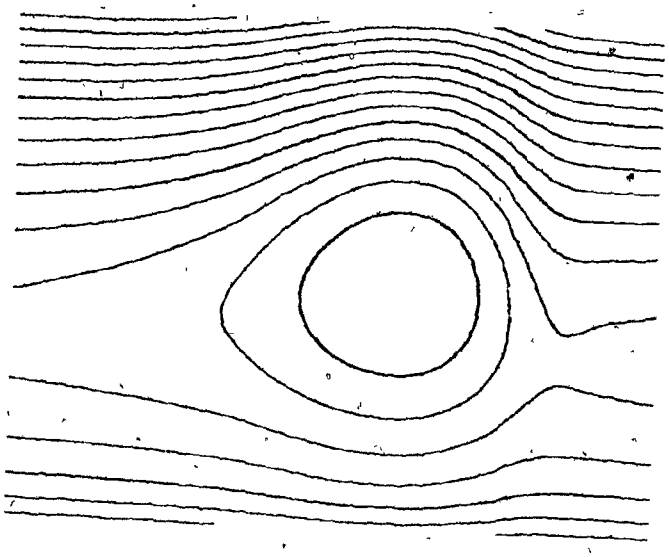

(E)

$\tau = 20$

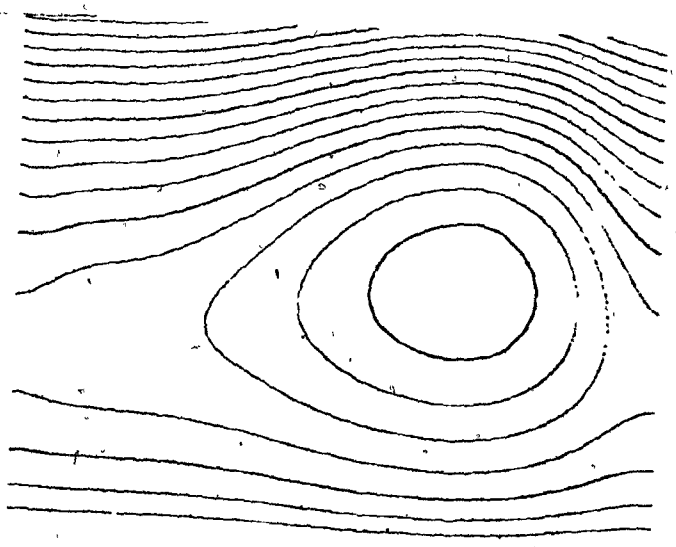

FIGURE 9 (CONTINUED)

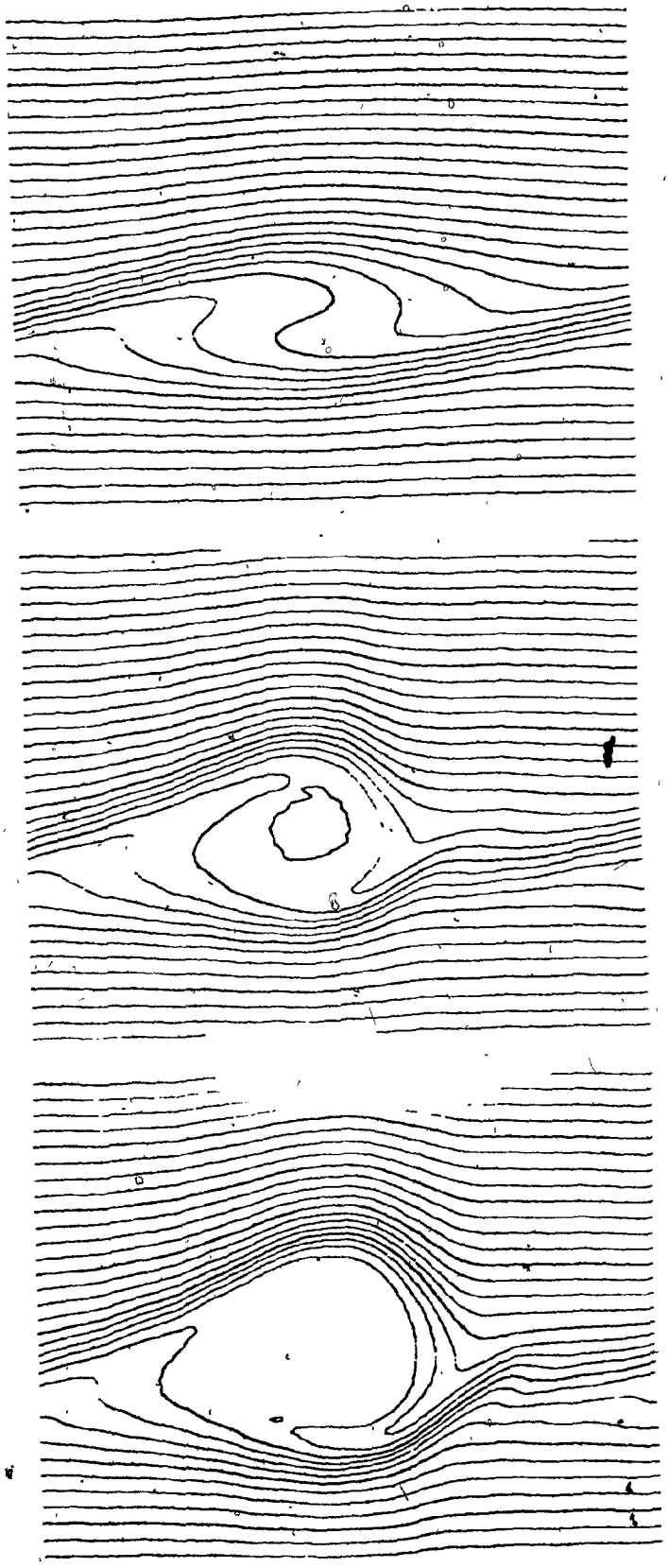

FIGURE 10

Absolute vorticity for curve 1 of figure 8

(D)

$\tau = 16$

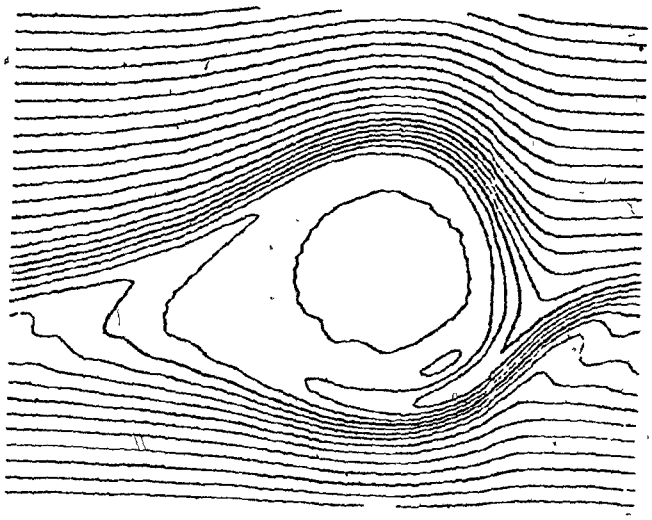

(E)

$\tau = 20$

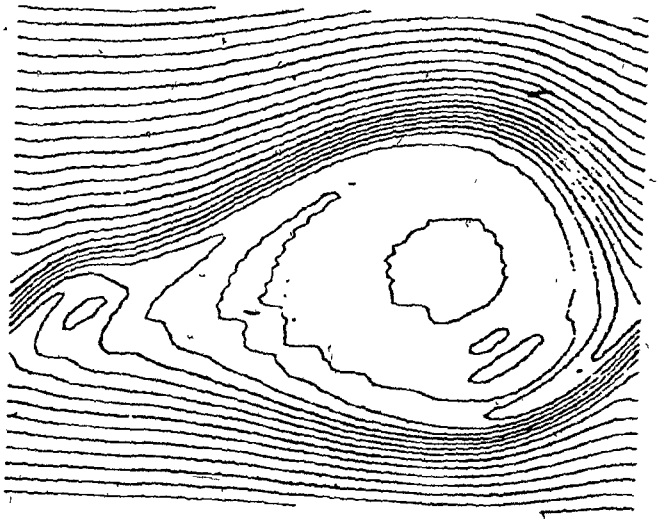

FIGURE 10 (CONTINUED)

It is also interesting to look at the total streamfunction and absolute vorticity fields for a run which is not quite resonant but is nearly steady in the latter stages. This is done in figures 11 and 12 which correspond to curve 10 of figure 6. The patterns are somewhat less intense than those just examined for the resonant case and they also demonstrate an additional feature. The Prandtl-Batchelor theorem (Batchelor, 1956) requires that the vorticity in the cat's eye be uniform in the steady state. Notice that this appears to be the case in figures 12(C) and 12(D).

(A)

$\tau = 4$

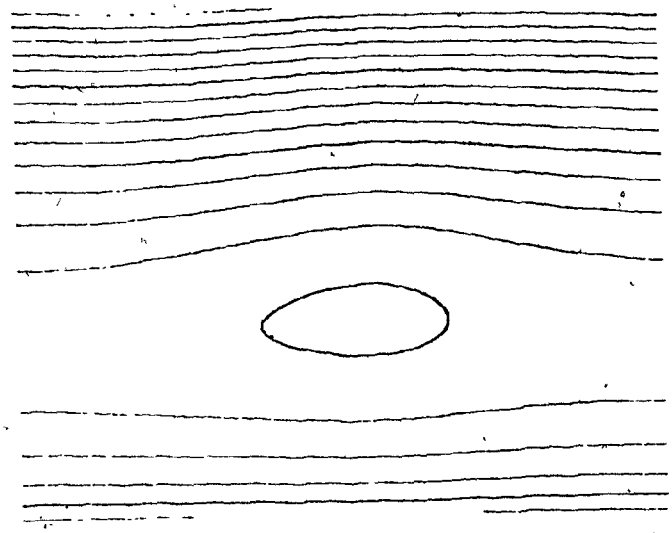

(B)

$\tau = 8$

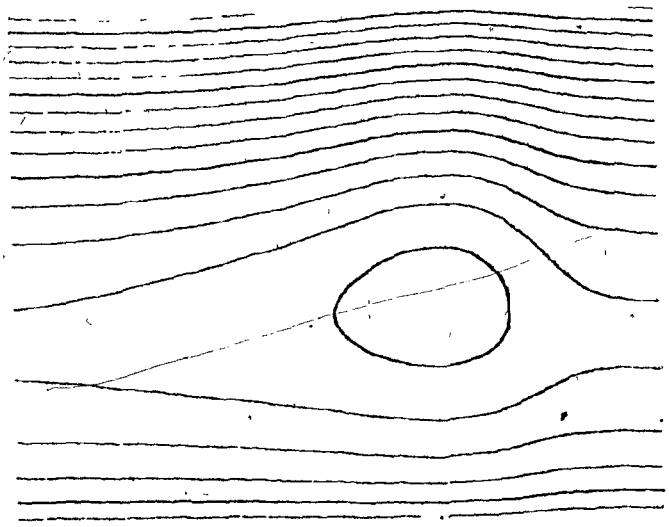

FIGURE 11

Total streamfunction for curve 10 of figure 6

(C)

$\tau = 12$

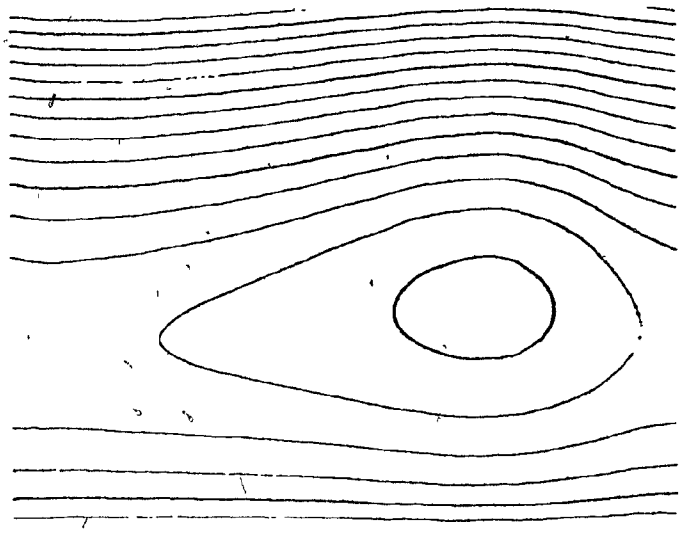

(D)

$\tau = 16$

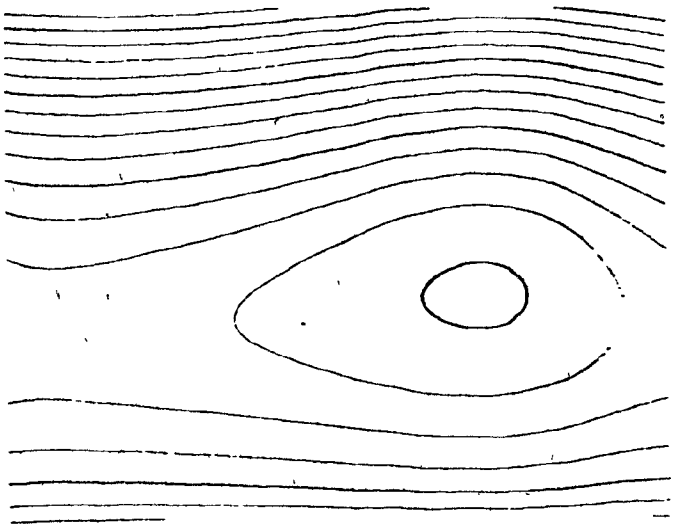

FIGURE 11 (CONTINUED)

(A)

$\tau = 4$

(B)

$\tau = 8$

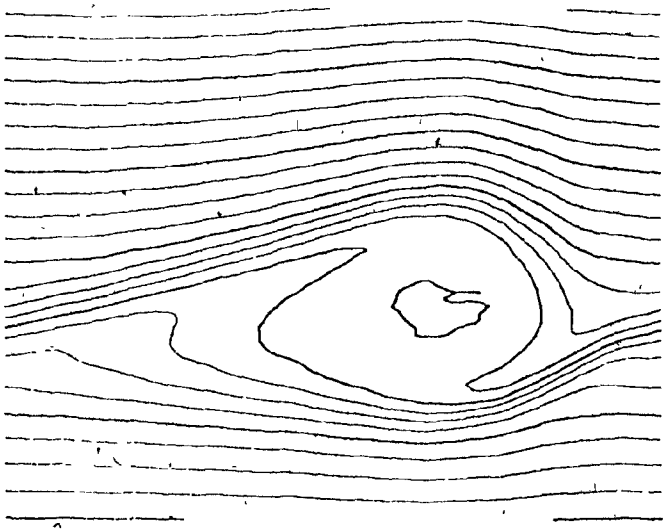

FIGURE 12

Absolute vorticity for curve 10 of figure 6

(C)

$\tau = 12$

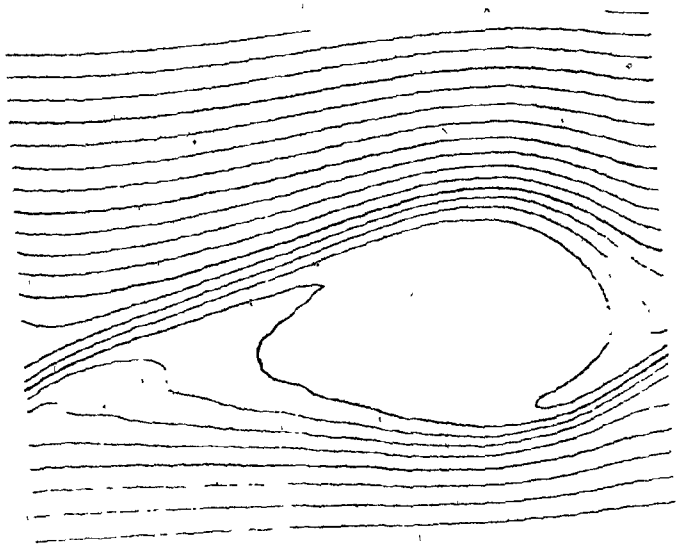

(D)

$\tau = 16$

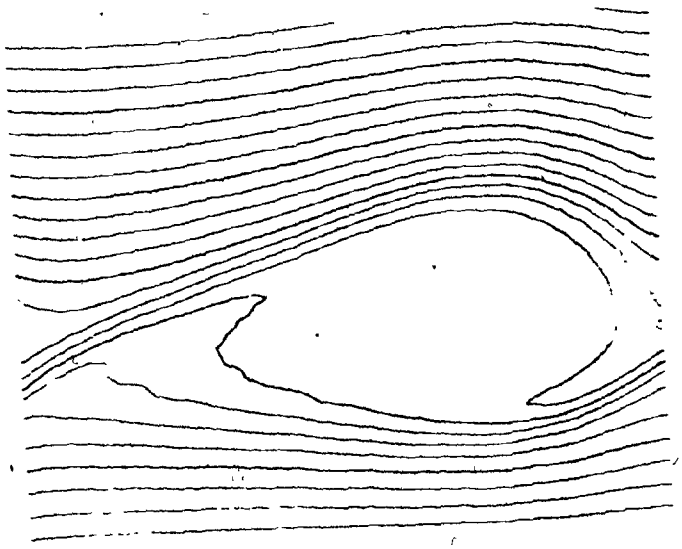

FIGURE 12 (CONTINUED)

CHAPTER 5. DISCUSSION

In the foregoing it has been demonstrated that, with the correct geometry and a nonlinear critical layer, it is possible to obtain a large response for weakly forced Rossby waves. It has also been found that during the amplification the critical layer expands to become a significant feature in the total flow pattern. Consequently, any scheme which attempts to model such a resonance will have to adequately simulate the nonlinear critical layer -- in particular it appears that it is a serious oversimplification to treat a critical layer as a reflecting surface in a linearized model.

The curves in figure 6(B) display an unexpected feature -- for these runs the most resonant case is initially the slowest growing. It appears that this behavior can be explained by the evolution of the imaginary part of the logarithmic phase shift.

It has also been shown (figure 8) that the time scale required to achieve a large response is strongly dependent on the relative strengths of the viscosity and nonlinearity. By changing from $\lambda = .5$ to $\lambda = .1$ the time required to produce a sevenfold amplification is decreased by a factor of two. Even for $\lambda = .1$, however, the time scale is very long compared to scales typical of synoptic meteorology processes. For example, choosing $U_s = 20$ m/s, $L = 500$ km., $\epsilon = .01$ and $\alpha = .4$ would give a dimensional time of 60 days corresponding to $\tau = 8$ in figure 8. Béland (1978) found that changing from $\epsilon \sim O(10^{-2})$ to $\epsilon = .1$ reduced the time scale for a related nonlinear process from 60 days to about a week.

This is an encouraging result but preliminary experiments indicate that for $\epsilon = .1$ the resolution requirements in the resonance problem are somewhat prohibitive. A more efficient method (e.g., the fast fourier transform) for calculating the nonlinear term would help in this regard.

APPENDIX : Approximation to the Transient Radiation Condition

The transient form of the southern boundary condition is

$$\frac{\partial \phi_n}{\partial y}(y,t) - \alpha n \, \phi_n(y,t) = -\int_0^t \phi_n(y,\tau)\, W_n(t-\tau)\, d\tau$$

$$= -\, I(t)$$

where

$$W_n(\xi) = \frac{\beta}{2\alpha} \, e^{-in\left(\bar{u} - \frac{\beta}{2\alpha^2 n^2}\right)\xi} \left\{ J_1\left(\frac{\beta}{2\alpha^2 n}\xi\right) + i\, J_0\left(\frac{\beta}{2\alpha^2 n}\xi\right) \right\}.$$

Let $\bar{\tau}$ be a fixed value of τ and $\phi_n(y, \bar{\tau})$ be the associated piece of streamfunction "history". The weight given to this history in the integral I(t) is $W_n(t-\bar{\tau})$, which will be different for each value of t; that is, the emphasis given to a particular piece of history changes as time goes on. This means that I(t) cannot be accumulated, but must be re-evaluated at each new time step -- a requirement which is very demanding on both execution time and storage for $\phi_n(y, \tau)$. Hence there is good reason to look for an approximation to I(t) in which at least a part of the integral can be accumulated. This can be achieved as follows :

Write $$I(t) = \underbrace{\int_0^{t-r} \phi_n(y,\tau)\, W_n(t-\tau)\, d\tau}_{(A)} + \underbrace{\int_{t-r}^{t} \phi_n(y,\tau)\, W_n(t-\tau)\, d\tau}_{(B)} .$$

In term (A), $r \le t-\tau \le t$; that is, the argument of the weighting function is larger than r. Using the asymptotic forms of Bessel functions J_0 and J_1 for large arguments leads to

$$W_n(t-\tau) \sim \sqrt{\frac{\beta n}{2\pi}} \frac{(-1+i)}{(t-\tau)^{1/2}} \left\{ e^{-in\bar{u}(t-\tau)} + O\left(\frac{1}{t-\tau}\right) \right\},$$

where we assumed $\frac{2\alpha^2 \eta}{\beta} \sim O(1)$.

Using a Taylor series expansion

$$(t-\tau)^{-1/2} = t^{-1/2} \left(1 - \frac{\tau}{t}\right)^{-1/2}$$

$$\doteq t^{-1/2} \left\{ \sum_{\ell=1}^{L} A_\ell \left(\frac{\tau}{t}\right)^{\ell-1} + O\left(\left\{\frac{\tau}{t}\right\}^L\right) \right\}$$

where $A_1 = 1$, $A_{\ell+1} = (1 - \frac{1}{2\ell}) A_\ell$ gives

$$W_n(t-\tau) \sim \sqrt{\frac{\beta n}{2\pi}} \frac{(+1+i)}{t^{1/2}} \left\{ \sum_{\ell=1}^{L} A_\ell \left(\frac{\tau}{t}\right)^{\ell-1} + O\left(\left\{\frac{\tau}{t}\right\}^L\right) \right\} \left\{ e^{-in\bar{u}(t-\tau)} + O\left(\frac{1}{t-\tau}\right) \right\}.$$

This result allows term (A) to be approximated as

$$\sqrt{\frac{\beta n}{2\pi}} \frac{(-1+i)}{t^{1/2}} e^{-in\bar{u}t} \sum_{\ell=1}^{L} \frac{A_\ell}{t^{\ell-1}} \int_0^{t-r} \phi_n(y,\tau)\, \tau^{\ell-1}\, e^{in\bar{u}\tau}\, d\tau.$$

Notice that t and τ have been separated and the integrals can be accumulated as time goes on. Thus a suitable approximation to I(t) is given by this approximation to term (A) plus term (B).

Evaluation of I(t) without making this approximation requires storage and integration over an interval of length t. Evaluation of the approximated version is much more efficient as it requires storage and integration over an interval of length r for term (B) plus a small overhead proportional to L for the approximation to term (A).

To test the approximation, two linear viscous runs were done for wavenumber 1 over 3000 time steps. In the first run I(t) was evaluated without making the preceding approximation, while in the

second the approximation to I(t) was used with r corresponding to 200 time steps and L = 20. The execution time, excluding calculation of the radiation condition, was about 30 seconds. Time spent calculating the radiation condition was about 17 seconds for the first run and 3 seconds for the second. The resulting values of the vorticity after 3000 time steps are given in table A. Comparing the results demonstrates that the approximation does not introduce significant error, even though it yields a considerable saving in execution time and storage requirements.

TABLE A : Vorticity after 3000 time steps

Y	No approximation to I(t) VORTICITY AMPLITUDE	PHASE(DEG)	With approximation to I(t) VORTICITY AMPLITUDE	PHASE(DEG)
2.243	.51089E+00	179.626	.51559E+00	179.626
2.043	.72624E+00	-176.730	.72622E+00	-176.730
1.843	.85752E+00	-162.499	.85753E+00	-162.499
1.643	.98343E+00	-152.094	.98342E+00	-152.093
1.443	.80563E+00	-138.910	.80566E+00	-138.910
1.250	.82041E+00	-141.291	.82045E+00	-141.291
1.099	.14390E+01	-118.392	.14390E+01	-118.393
.977	.96781E+00	-117.203	.96787E+00	-117.205
.894	.19853E+01	-95.787	.19853E+01	-95.788
.810	.14291E+01	-67.921	.14291E+01	-67.924
.748	.13673E+01	-61.118	.13674E+01	-61.122
.694	.20577E+01	-66.199	.20578E+01	-66.202
.646	.27446E+01	-88.019	.27447E+01	-88.021
.602	.20825E+01	-115.158	.20826E+01	-115.160
.560	.11819E+01	-59.487	.11820E+01	-59.492
.520	.31278E+01	-70.162	.31278E+01	-70.164
.480	.24398E+01	-106.480	.24399E+01	-106.482
.440	.16374E+01	-39.996	.16373E+01	-40.000
.400	.40572E+01	-63.891	.40572E+01	-63.892
.360	.26782E+01	-100.633	.26783E+01	-100.635
.320	.26073E+01	-22.220	.26073E+01	-22.223
.280	.56135E+01	-57.404	.56135E+01	-57.405
.240	.29057E+01	-93.098	.29058E+01	-93.100
.200	.46141E+01	-7.181	.46139E+01	-7.182
.160	.90754E+01	-50.349	.90754E+01	-50.350
.120	.34203E+01	-82.546	.34204E+01	-82.549
.080	.13220E+02	7.921	.13219E+02	7.920
.040	.31289E+02	-43.743	.31289E+02	-43.743
-.000	.63670E+02	75.680	.63670E+02	75.680
-.040	.25399E+02	-157.543	.25399E+02	-157.542
-.080	.11022E+02	130.741	.11022E+02	130.742
-.120	.17829E+01	-31.292	.17829E+01	-31.296
-.160	.54467E+01	-157.688	.54469E+01	-157.687
-.200	.36340E+01	124.123	.36345E+01	124.125
-.240	.11816E+01	-36.124	.11816E+01	-36.133
-.280	.28746E+01	-158.691	.28747E+01	-158.690
-.320	.21284E+01	117.507	.21283E+01	117.513
-.361	.85285E+00	-37.570	.85283E+00	-37.583
-.403	.15479E+01	-148.118	.15481E+01	-148.116
-.450	.13324E+01	147.974	.13324E+01	147.981
-.503	.88273E+00	101.046	.88266E+00	101.054
-.567	.62081E+00	89.051	.62073E+00	89.059
-.646	.46386E+00	131.367	.46386E+00	131.379
-.755	.24516E+00	-126.130	.24627E+00	-126.133
-.920	.21315E+00	132.808	.21315E+00	132.842
-1.183	.10921E+00	56.585	.10890E+00	56.633
-1.552	.20371E+00	104.169	.20336E+00	104.371

BIBLIOGRAPHY

Ahlberg, J., E. Nilson and J. Walsh, 1967: The Theory of Splines and Their Applications. Academic Press, 284 pp.

Batchelor, G. K., 1956: On steady, laminar flow with closed streamlines at large Reynolds number. J. Fluid Mech., 1, 177-190.

Béland, M., 1976: Numerical study of the nonlinear Rossby wave critical level development in a barotropic zonal flow. J. Atmos. Sci., 33, 2066-2078.

_____, 1978: The evolution of a nonlinear Rossby wave critical level: effects of viscosity. Submitted J. Atmos. Sci.

_____, and T. Warn, 1975: The radiation condition for transient Rossby waves. J. Atmos. Sci., 32, 1873-1880.

Benney, D. J., and R. F. Bergeron, 1969: A new class of nonlinear waves in parallel flows. Stud. Appl. Math., 48, 181-204.

Brown, S. N., and K. Stewartson, 1978: The evolution of the critical layer of a Rossby wave. Part II. Geophys. Astrophys. Fluid Dyn., Vol. 10, 1-24.

Cullen, M., 1976: On the use of artificial smoothing in Galerkin and finite difference solutions of the primitive equations. Quart. J. Roy. Meteor. Soc., 102, 77-93.

Davis, R. E., 1969: On the high Reynolds number flow over a wavy boundary. J. Fluid Mech., 36, 337-346.

Dickinson, R. E., 1968: Planetary Rossby waves propagating vertically through weak westerly wind wave guides. J. Atmos. Sci., 25, 984-1002.

_____, 1970: Development of a Rossby wave critical level. J. Atmos. Sci., 27, 627-633.

Haberman, R., 1972: Critical layers in parallel flows. Stud. Appl. Math., 51, 139-160.

Lin, C., 1967: The Theory of Hydrodynamic Stability. Cambridge Univ. Press, 155 pp.

Staniforth, A., and R. Daley, 1977: A finite-element formulation for the vertical discretization of sigma-coordinate primitive equation models. Mon. Wea. Rev., 105, 1108-1118.

Staniforth, A., and H. Mitchell, 1977: A semi-implicit finite-element barotropic model. Mon. Wea. Rev., 105, 154-169.

_____, 1978: A variable resolution finite-element technique for regional forecasting with the primitive equations. Mon. Wea. Rev., 106, 439-447.

Strang, G., and G. Fix, 1973: An Analysis of the Finite Element Method. Prentice Hall, 306 pp.

Stewartson, K., 1978: The evolution of the critical layer of a Rossby wave. Geophys. Astrophys. Fluid Dyn., Vol. 9, 185-200.

Tung, K., 1977: Stationary atmospheric long waves and the phenomena of blocking and sudden warming. Ph.D. thesis, Harvard University, Cambridge, Massachusetts.

Warn, T., and H. Warn, 1976: On the development of a Rossby wave critical level. J. Atmos. Sci., 33, 2021-2024.

_____, 1978: The evolution of a nonlinear critical level. To appear in Stud. Appl. Math.